Extreme humid heat in South and Southeast Asia in April 2023, largely driven by climate change, detrimental to vulnerable and disadvantaged communities

1. Mariam Zachariah, *Grantham Institute, Imperial College London, UK*
2. Robert Vautard, *Institut Pierre-Simon Laplace, CNRS, Sorbonne Université, Paris, France*
3. Chaithra S T, *Centre for Atmospheric Sciences, Indian Institute of Technology Delhi, India*
4. Joyce J Kimutai, *Grantham Institute, Imperial College London, UK*
5. Arulalan T, *India Meteorological Department, Ministry of Earth Sciences, Gov. of India, Centre for Atmospheric Sciences, Indian Institute of Technology Delhi, India*
6. Krishna AchutaRao, *Centre for Atmospheric Sciences, Indian Institute of Technology Delhi, India*
7. Clair Barnes, *Grantham Institute, Imperial College London, UK*
8. Roop Singh, *Red Cross Red Crescent Climate Centre, The Hague, the Netherlands*
9. Maja Vahlberg, *Red Cross Red Crescent Climate Centre, The Hague, the Netherlands*
10. Julie Arrgihi, *Red Cross Red Crescent Climate Centre, The Hague, the Netherlands; Global Disaster Preparedness Center, Washington DC, USA; University of Twente, The Netherlands*
11. Emmanuel Raju, *Department of Public Health, Global Health Section & Copenhagen Centre for Disaster*
12. Upasna Sharma, *School of Public Policy, Indian Institute of Technology Delhi, India*
13. Anshu Ogra, *School of Public Policy, Indian Institute of Technology Delhi, India*
14. Chaya Vaddhanaphuti, *Department of Geography, Faculty of Social Sciences, Chiang Mai University, Thailand*
15. Chandra Sekhar Bahinipati, *Department of Humanities and Social Sciences, Indian Institute of Technology Tirupati, India*
16. Petra Tschakert, *School of Media, Creative Arts and Social Inquiry, Curtin University, Perth, Australia*
17. Ram Chandrasekaran, *School of Media, Creative Arts and Social Inquiry, Curtin University, Perth, Australia*
18. Carolina Pereira Marghidan, *Red Cross Red Crescent Climate Centre, The Hague, the Netherlands; Faculty of Geo-Information Science and Earth Observation (ITC), University of Twente, Enschede, the Netherlands*
19. Arpita Mondal, *Civil Engineering Department, Indian Institute of Technology Bombay, India; IDP in Climate Studies, Indian Institute of Technology Bombay, India*
20. Clemens Schwingshackl, *Department of Geography, Ludwig-Maximilians-Universität München, Munich, Germany*
21. Sjoukje Philip, *Royal Netherlands Meteorological Institute (KNMI), De Bilt, The Netherlands*
22. Sarah Kew, *Royal Netherlands Meteorological Institute (KNMI), De Bilt, The Netherlands*
23. Friederike E L Otto, *Grantham Institute, Imperial College London, UK*

https://doi.org/10.25561/104092

Main findings

- Heatwaves are amongst the deadliest natural hazards with thousands of people dying from heat-related causes each year and many more suffering other severe health and livelihood consequences. However, the full impact of a heatwave is often not known until weeks or months later, once death certificates are collected, or scientists can analyse excess deaths. Many places lack good record keeping of heat-related deaths, therefore currently available global mortality figures are likely an underestimate.

- While people in the affected regions are used to hot and humid temperatures, those who are more physiologically susceptible to heat (e.g. due to pre-existing conditions, age, disability etc.) and/or are more exposed due to their occupation (e.g. outdoor workers, farmers) are at highest risk of heat-related health impacts. Such exposure and vulnerability are intensified by societal disadvantage based on factors such as socio-economic status, religion, caste, gender, migration, and living conditions. On top of this, factors such as air pollution, the urban heat island effect, and wildfires further compound health impacts, particularly among the most vulnerable populations.

- In the current climate, which has warmed by 1.2°C since pre-industrial times due to human activities, the humid heat event (defined using the heat index) is not very unusual over India and Bangladesh, but is estimated to be rare in Thailand and Lao PDR.

- The estimated heat index values exceeded the threshold considered as “dangerous” (41°C) over the large parts of the South Asian regions studied. In a few areas, it neared the range of “extremely dangerous” values (above 54°C) under which the body temperature is difficult to be maintained.

- There is only one data set available for the entire region to calculate the heat index (ERA5). This dataset is known to underestimate extreme temperature trends over India, so the estimates for the rarity and severity of the event are more uncertain than when several datasets can be compared.

- To estimate the influence that human-caused climate change has had on extreme heat since the climate was 1.2°C cooler, we combine climate models with observations. Observations and models both show a strong increase in likelihood and intensity of April humid heat events similar to that of 2023.

- The combined results give an increase in the likelihood of such an event to occur of at least a factor of 30 over India and Bangladesh due to human-induced climate change. At the same time, a heatwave with a chance of occurrence of 20% (1 in 5 years) in any given year over India and Bangladesh is now about 2°C hotter in heat index than it would be in a climate not warmed by human activities.

- Over Thailand and Lao PDR, a humid heatwave with a 0.5% chance of occuring in any given year (1 in 200 years) is now 2.3°C hotter in heat index. An event of the same magnitude as the observed heatwave would have been extremely rare in a 1.2°C cooler climate and hence it would have been virtually impossible to have occurred without climate change.

- These trends will continue with further warming. They are stronger for the rarer event over Thailand and Lao PDR where a heatwave like the recent event would be about 10 times more likely in a 0.8°C warmer world (2°C global warming since pre-industrial times). In India and Bangladesh, the likelihood of this April's event reoccuring would increase by about a factor of 3 between today and reaching 2°C global warming, meaning that this humid heat event could be expected every 1-2 years.

- There are a range of solutions to heat-related harms from the individual to the regional level. They are currently implemented as patchwork, to various degrees, across the countries studied, with India having the most advanced heatwave planning. Solutions, such as self-protective action, early warning systems for heat, passive and active cooling, urban planning, and heat action plans can be effective at reducing fatalities and other negative impacts. In fact, heat-related fatalities have decreased in regions where heat action plans have been in place, e.g. in the city of Ahmedabad and the region of Odisha in India. However, these solutions are often out of reach for the most vulnerable people, highlighting the need to improve vulnerability assessments and design interventions that account for group-specific needs.

- High social vulnerability among various segments of society, in combination with the strong increase in extreme heat in the region, is likely to exacerbate the impacts of extreme heat events on those already experiencing substantial disadvantages in their daily lives and hence requires comprehensive adaptation and development interventions.

1 Introduction

Prolonged heatwave conditions prevailed from the second to fourth week of April 2023 over South and Southeast Asia, when the majority of Bangladesh, India, China, Thailand, and Lao PDR experienced record-breaking temperatures (The Guardian, 2023; The Diplomat, 2023; CNN, 2023; USA Today, 2023; Arab News, 2023; Vox, 2023; Hindustan Times, 2023; The Straits Times, 2023). On 16th April, Dhaka (Bangladesh) observed 40.6°C (Arab News, 2023), which is the highest maximum temperature recorded in decades, leading to sudden increases in heat stroke cases, melting roads, and a strong surge in electricity demand throughout the country (The Guardian, 2023; Hindustan Times, 2023). In India, Pragyaraj (Uttar Pradesh) reached 44.6°C on 17 April (The New Indian Express, 2023) and several Northern and Eastern cities recorded maximum temperatures above 44°C on 18th of April (The Guardian, 2023). That same week, schools in Tripura and Odisha states remained closed to limit students' exposure to the extreme heat (The Hindu,2023; The Guardian, 2023; Zeebiz, 2023), and in the West Bengal, the local government preponed summer vacations by three weeks (Times Now, 2023). According to the Indian Meteorological Department (IMD), the temperatures were hovering between 40°C and 44°C over parts of North, Central and East India from 16th to 20 April. On the 16th of April, 13 fatalities and about 650 hospitalisations were recorded in the city of Navi Mumbai (Maharashtra) due to heat strokes (The Guardian, 2023; AccuWeather, 2023; The Independent, 2023; Mint, 2023; The Straits Times, 2023).

Thailand recorded its highest ever temperature of 45.4°C on 15th April in the city of Tak, breaking the previous all-time record of 44.6°C in Mae Hong Son on 28 April 2016 (The Washington Post, 2023; The Independent, 2023; Japan Times, 2023; The Guardian, 2023) by 0.8°C. According to news reports, the heatwave caused power outages in several parts of Thailand as well as casualties, including a traffic police officer reportedly suffering a heat-induced heart attack in the province of Samut Prakan (AP News, 2023). According to the national weather service of Thailand, the heat index (a measure of what the temperature 'feels like' to humans, accounting for air humidity) hit a record of 54°C. The Sainyabuli province in Lao PDR reported 42.9°C on 20th April as their all-time national temperature record (Independent, 2023). Vientiane, the capital of Lao PDR, recorded 41.4°C on 15th April, the hottest day ever for the capital. On 18 April, Luan Prabang in Lao PDR even reported 42.7°C (CNN, 2023).

The impacts of the heatwave were further exacerbated by other hazards occurred during this heatwave season. There have been reports of 1,156 forest fires across India between 13 and 20 February 2023 (NASA's Fire information for Resource Management). These fires caused severe damage to forest ecosystems and people whose livelihoods depend on forests and led to severe air pollution. Raging forest fires in Thailand in March 2023 have substantially worsened the country's air pollution, causing nearly 2 million people to go to hospitals with respiratory illnesses (Japan Times, 2023).

These high levels of air pollution were maintained over a long time due to stagnant conditions in many South and Southeast Asian cities (Dhaka Tribune, 15 April 2023; The Guardian, 17 April 2023). In such polluted urban areas, heat can amplify the negative impacts of aerosols and other atmospheric pollutants (Touchaei *et al.*, 2016). For example, the intricate gas chemistry over the urbanised areas tends to amplify ozone production (Wu *et al.*, 2019), as well as secondary organic aerosols, leading to the deterioration of regional air quality during extremely hot days and thus further exacerbating the effects of heatwaves on human health.

Even without high levels of air pollution heatwaves have a strong effect on human health. At elevated temperatures, the human body regulates its core temperature through sweating. If the warm air is also humid, it restricts evaporation of sweat from the body, causing core body temperature to continue to rise. This leads to further loss of moisture through sweat as the body attempts to cool, thus leading to dehydration, fatigue and in some cases death due to heat stroke. Outlooks from national weather services in the affected countries have begun to incorporate 'feels like' or apparent temperature in addition to the near-surface air temperature (see e.g. India Meteorological Department; The Economic Times, 2023; Thailand Meteorological Department (*in Thai*); Sky News, 2023). One commonly used metric is the Heat Index (HI), which integrates temperature and humidity to provide temperature estimates that are reflective of the human body's comfort to the combined effects of temperature and humidity (see Section 2.3 for more details on the Heat Index). HI has been used in particular in the AR6 WGI report to show the influence of climate change on the number of days of dangerous heat conditions in many tropical areas (Ranasinghe *et al.*, 2021; see Figure 12.4). HI quantifies the risk of heat potentially causing heat-related disorders in people, with higher values indicating higher risks. The HI values are categorised as (Blazejczyk *et al.*, 2012; Debnath *et al.*, 2023).

- < 27 °C: Low risk
- 27–32 °C: Caution
- 32–41 °C: Extreme caution
- 41–54 °C: Danger
- > 54 °C: Extreme danger

In this study, we focus on four countries - India, Bangladesh, Thailand, and Lao PDR - where temperature records were broken at several locations during the heat event in April 2023, and heat-related casualties were reported. The health impacts associated with the heatwave occurred after relatively short exposure to extreme heat, but the heatwave peaked at slightly different times across the region. To capture the highest temperatures across the study region, the event is therefore defined as the

https://doi.org/10.25561/104092

4-day mean of the daily HI values.. Due to the heterogeneity in climate and terrain over this large area, it is separated into two smaller homogeneous regions as follows:

i. The tropical regions of south and central India and the whole of Bangladesh. This domain is delineated based on the Köppen-Geiger climate classification, excluding the dry, semi-arid region that runs parallel to the Western Ghats where humidity is low in the pre-monsoon season. Fig. 1(a) shows the maximum 4-day average HI during 17-20 April, 2023 over this domain (hereafter the IB region; highlighted by the outer blue boundary, but excluding the filled polygon that masks the dry region).

ii. Thailand and Lao PDR together, hereafter the TL region, as shown by the blue boundary in Fig. 1(b). The highest 4-day HI in this region occurred on 18-21 April, 2023.

Fig. 1(c-d) shows the heat risk according to HI in the IB and TL regions, respectively. In both the study regions, the heat index values are found to be at ‘Danger’ level over large areas. In several urban locations, the heat index values even reached values indicating ‘Extreme danger’ at different times during the 4-day period.

https://doi.org/10.25561/104092

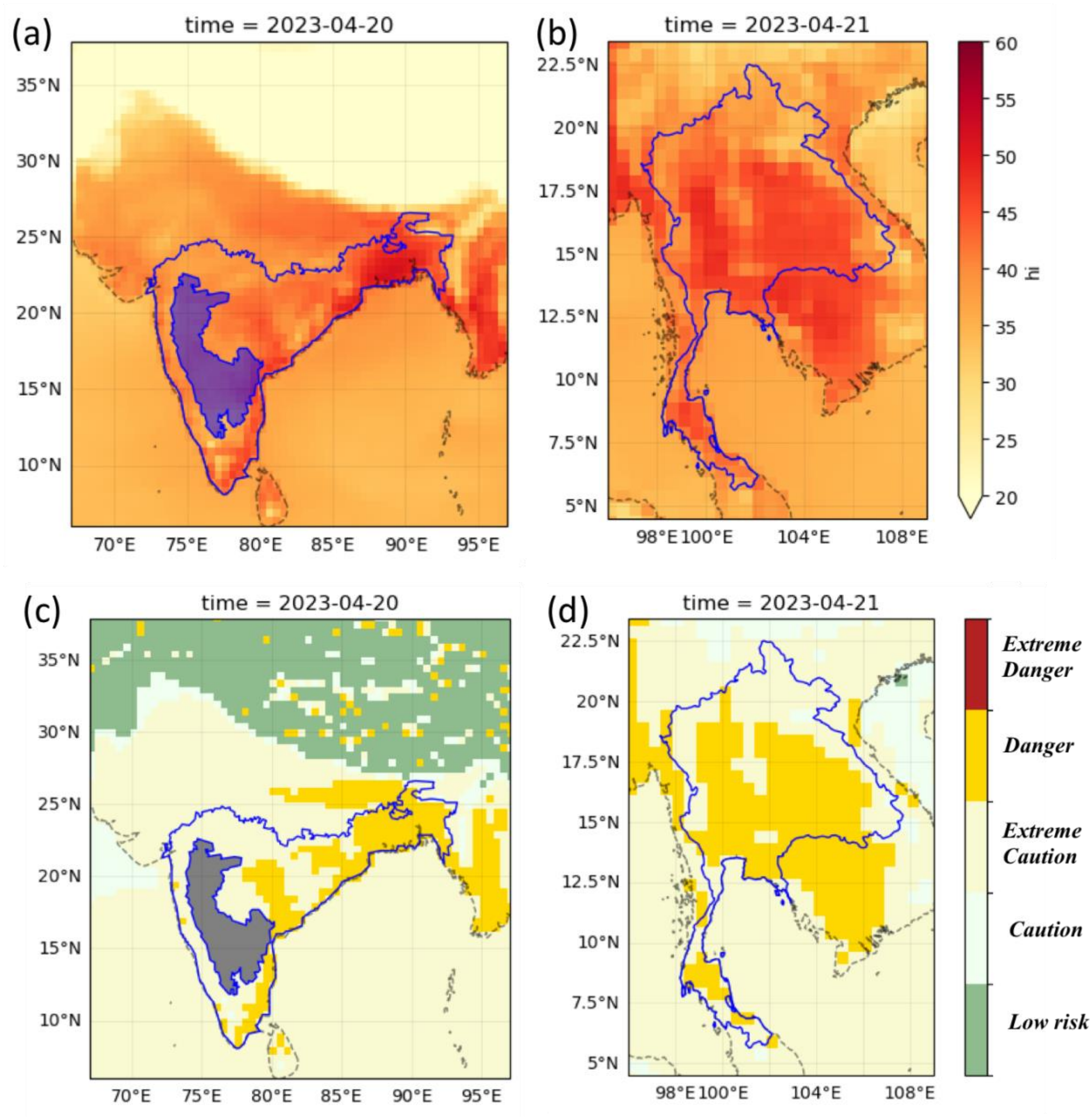

Figure 1*: (a) Heat Index (calculated from ERA5 near-surface temperature and dew point temperature) [°C] showing 4-day average daily maximum for the period from 17th to 20th of April 2023 for the India-Bangladesh region (outlined in blue). The dry, semi-arid region along the rain-shadow of the Western Ghats in India, as shown by the filled polygon is excluded from the analysis as the impacts defined by the combination of high humidity and high temperatures is not applicable in this region. (b) 4-day average daily maximum Heat Index during 18-21 April, 2023, over the Thailand-Lao PDR region (outlined in blue). c) Classification maps for heat impacts based on HI, for the 4-day average daily maximum HI for the period 17-20 April, 2023 for the India-Bangladesh region. (d) Classification maps for heat impacts based on HI, for the 4-day average daily maximum HI for the period 18-21 April, 2023, over the Thailand-Lao PDR region*

https://doi.org/10.25561/104092

1.1 South and Southeast Asia climate

There are a limited number of studies on extreme heat in Southeast Asia. Overall, under increasing global warming, the region is expected to experience heatwaves more frequently, of longer duration, and with higher temperatures (Dong *et al.*, 2021; Sun *et al.*, 2022). The increase in population exposure to extreme temperature in Southeast Asia is estimated to be about 590 million person-days, although there are great variations within the subregions (Sun, 2022; Fig.2 shows the number of heat-related deaths in selected South Asian countries).

In the context of India, Mazdiyasni *et al.* (2017) observed a positive causal association between number of heatwave days and human casualties. Kumar *et al.* (2016) estimated both direct and indirect economic loss and damages (L&Ds) from heatwaves in two districts of Odisha in 2014, amounting to USD 135 (INR 11,107) and USD 15 (INR 1191) per household, respectively. According to Ray *et al.* (2021), heatwaves were the third largest contributor to mortality in India between 1970-2019, contributing about 12% of all mortalities due to extreme weather events. During the same period, heat-related mortality increased by 62% in India, and the states of Andhra Pradesh and Odisha had the highest mortality rate per year per million population at 3.3 and 1.0, respectively (Ray *et al.*, 2021). A study by Kumar and Singh (2021) confirms that there has been a statistically significant increase in heat-related deaths in India, from 3863 cases in 2001-2005 to 6411 cases in 2011-2015. Currently, Uttar Pradesh and Andhra Pradesh have the highest number of deaths. Further, Das (2015) found that additional expenditures for urban informal workers have increased by USD 1,22 (INR 100) per heatwave day. From 1992 to 2020, heatwaves caused mortality of around 26,355 in India, and more than 3000 deaths occurred in the year 1998 (see Fig. S1).

South and Southeast Asia are both identified as highly vulnerable to climate change impacts because of the region's geography and climate, with high temperature and humidity year-round (Im et al., 2017; Revadekar et al.,2012). In addition, rapid urbanisation, dense and growing population with poverty, inequality and poor health infrastructure can exacerbate this vulnerability (Pal and Eltahir 2016; Arshad et al 2020; Ullah et al 2022). Much of the population's livelihood is dependent on agriculture, exposing a large proportion of the population to outdoor temperatures (Dash and Kjellstrom 2011;). Extreme temperatures remain a major threat over this part of the Asian continent, putting millions at risk (NRDC, 2022). The rise in humidity with global warming, particularly in regions with warm and humid weather, can exacerbate the health dangers associated with extreme temperatures. Even though geographical and climatological features play an important part in modulating impacts related to extreme temperatures, the magnitude and pattern of mortality are significantly influenced by local factors such as demographics, socio-economic status, underlying health conditions, built environment, etc (Cissé, G., et al. 2022; Jones et al.,2018; Uejio et al.,2011; Hajat and Kosatky 2010; Xu et al.,2013).

South Asia comprises about 24% of the world's population and has dry temperate, tropical climates under the Köppen–Geiger classification (Kottek *et al.*, 2006). The South Asian region is characterised by diverse geographical features consisting of rainforests, deserts, high-altitude glaciers, grasslands and valleys. The climate of these regions differs substantially and is modulated by factors such as monsoon, altitude and proximity to the coast (Peel *et al.*, 2007).

The southern parts of Asia are particularly vulnerable to longer and more deadly heatwaves (Colvin and McDonagh, 2017; Alessandro Dosio *et al.*, 2018; Im *et al.*, 2017; Dong *et al.*, 2021). The annual mean temperature over many parts of South Asia has increased in recent decades (Coumou *et al.*, 2013).

https://doi.org/10.25561/104092

Projections over this region indicate significant increase in frequency and intensity of temperature extremes with emphasis on severe robust changes over northwest India, southwest Afghanistan and the deserts region in Pakistan (De *et al.*, 2005; Sidiqi *et al.*, 2018). Some of the most severe historical heat episodes in the southern Asian region, which led to thousands of human and livestock casualties, occurred in 1998 (De and Mukhopadhyay, 1998; Jenamani, 2012) over eastern India, in 2003 in Andhra Pradesh (Bhadram *et al.*, 2005), in 2015 in large parts of South Asia (Wehner *et al.*, 2016; Masood *et al.*, 2015) and most recently in 2022 hitting large parts of India and Pakistan (Zachariah *et al.*, 2022). The 2015 heatwave had devastating impacts on many countries in South Asia with the death toll reaching about 3500 (Guha-Sapir *et al.*, 2016; Im *et al.*, 2017).

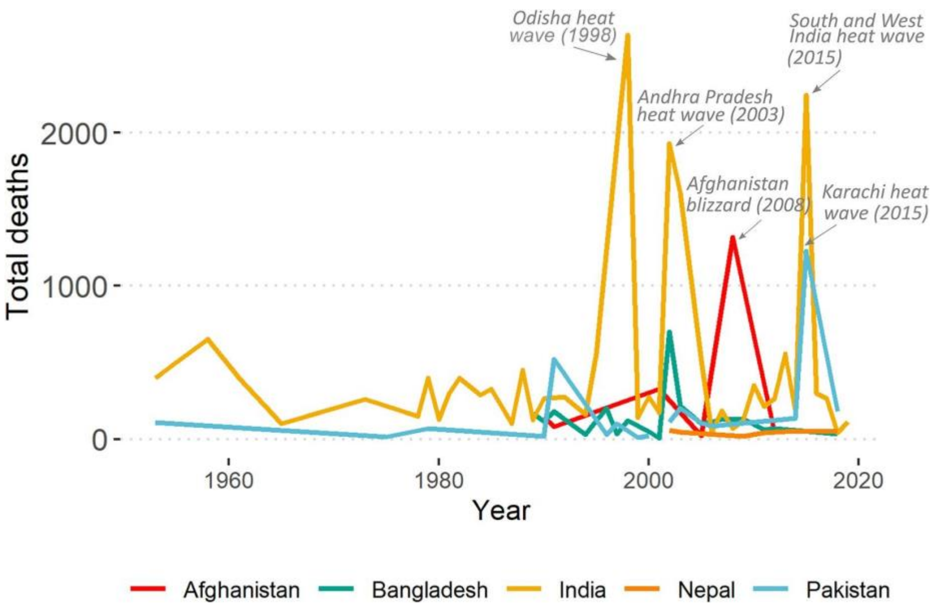

Figure 2 *:* Deaths caused by extreme temperature events in South Asia (Dimitrova *et al.*, 2021)

The recurrent heatwaves experienced by South Asian regions in the past few decades are due to the diverse geography along with changes in regional circulation patterns and variations in sea surface temperatures (Mani *et al.*, 2018). Apart from these, inter-annual monsoon variability is also found to be linked to heatwave occurrence over South Asia (Satyanarayana and Rao, 2020). For instance, the presence of subtropical highs over the Tibetan plateau for an extended period of time leads to dry weather conditions and the occurrence of heatwaves (McGregor and Nieuwolt 1998). Warm air masses and airflow patterns are produced in these regions distributing hot air. This results in increased insolation and anticyclonic flow along with dry weather conditions (Jenamani, 2012). Concurrent dry weather conditions during the summer season and reduction in rainfall in southwestern Pakistan, western India and Bangladesh are notable drivers for drought and heatwaves in these regions.

The climate of southeast Asia is primarily modulated by both Asian and Australian monsoon systems (Chang *et al.*, 2005). ENSO is also found to be an important planetary-scale climate forcer influencing the rainfall and temperature over southeast Asia on an interannual timescale (Wang *et al.*, 2003; Yuan and Yang, 2012; Marlier *et al.*, 2012; Wooster *et al.*, 2012). Although there is a limited variation in seasonal temperatures over these regions, heatwaves still severely affect the local population. From 1998 to 2008 an increasing number of deaths were reported in central and northern Thailand from heat related events (Huang *et al.*, 2018). The April 2016 extreme heat event over southeast Asia broke the temperature record dating back to the mid-twentieth century (Thirumalai *et al.*, 2017). During this event,

https://doi.org/10.25561/104092

Thailand saw a new record of temporal heat extent after 1950 with one day reaching 44.3°C and maximum temperature in each day of April exceeding 40°C.

In East Asia, heatwaves primarily result from enhanced near-surface air temperature resulting in movement of warm air due to warm-core low pressure in the lower troposphere (Luo *et al.*, 2020). The circulation changes during ENSO events combined with reduced rainfall add to increased intensity, frequency and duration of heatwaves over southeast Asia (Luo and Lau, 2017). Im *et al.* (2017) identified three mechanisms contributing to hot and humid conditions (quantified by wet-bulb temperature), thereby enhancing heatwave conditions over south Asia. First, warm and humid air masses from the Arabian Sea and Bay of Bengal are brought into the Indus and Ganges valleys by the monsoon system. The second reason is the warmer surface air conditions in the low surface elevated regions (generally <100m) than the neighbouring high-elevated areas. Lastly, irrigation in these valleys modifies the surface energy balance resulting in enhanced wet-bulb temperatures.

Extreme temperatures have shown a robust global increase since 1950 (Seneviratne *et al.*, 2021). Observations reveal clear increase in intensity and frequency of hot days over the Asian regions in the recent decades (Dunn *et al.*, 2020) and it is very likely that this observed trend is attributable to human-induced climate change (Hu *et al.*, 2020; Seneviratne *et al.*, 2021; Seong *et al.*, 2021). Imada *et al.* *(*2018) observe that the spatial coverage of extreme warmth has increased over Asian regions in the 1951-2016 period. Observational evidence points to significant increases in the intensity and frequency of hot extremes over south Asia (Sheikh *et al.*, 2015; Rohini *et al.*, 2016; Ratnam *et al.*, 2016; Dimri, 2019) as well as Southeast Asia (Supari *et al.*, 2017; Cheong *et al.*, 2018; Dunn *et al.*, 2020). Climate models project increases in the frequency and intensity of extreme temperatures under global warming over Asia (Sillmann *et al.*, 2013a; Sillmann *et al.*, 2013b; Xu *et al.*, 2017; Li *et al.*, 2019) with increased intensity, frequency and duration of heatwaves projected over India (Murari *et al.*, 2015; Mishra *et al.*, 2017; Rohini *et al.*, 2019; Das *et al.*, 2021) and Pakistan (Nasim *et al.*, 2018; Ali *et al.*, 2019; Khan *et al.*, 2020). A recent study by Arulalan *et al.*, (2023) examined future heatwaves over India with a large set of model simulated datasets (1500 ensembles), and found that the shorter duration heatwave events (3–5 days long) are 2–10 times more probable in the + 1.5 °C and + 2 °C futures, whereas longer events (7 and 9 days) increase by a factor of 10–30. Also, the area likely to experience long duration heatevents in future extends into regions previously not prone to such heatevents. Thus, heatwaves of the future are therefore likely to be more widespread in area and of longer durations in India.

2 Data and methods

2.1 Observational data

We use three gridded datasets for fitting probability distributions to variables of interest in the study regions and for analysing the heatwave event in the context of climate change. The first dataset is the ERA5 reanalysis product (Hersbach *et al.*, 2020), extracted at daily time steps for the period January 1, 1950 - April 27, 2023. The 2m air temperature and dew point temperature that are required for estimating the daily maximum temperature and relative humidity variables needed for calculating the HI (see section 2.3), were downloaded at 0.5º resolution from ECMWF. The second dataset is the CPC gridded dataset for daily maximum temperature provided by the NOAA/OAR/ESRL Physical Sciences Laboratory, Boulder, Colorado, USA. This product is available as daily data at 0.5° x 0.5° resolution for the period January 1, 2015 - present. For validating these datasets, we use gridded datasets of observed daily maximum temperature at 1° x 1° resolution for the period from January 1, 1951 to April

30, 2023, provided by the Indian Meteorological Department (IMD; Srivastava *et al.*, 2009), as an additional observational product. Its spatial extent is limited to within the geographical borders of India.

Among these datasets, only ERA5 provides dew point temperatures, which are needed for estimating relative humidity (RH) and in turn, calculate HI over both study regions (see Section 2.3 for details of HI computation).

As a measure of anthropogenic climate change, we use the (low-pass filtered) global mean surface temperature (GMST), where GMST is taken from the National Aeronautics and Space Administration (NASA) Goddard Institute for Space Science (GISS) surface temperature analysis (GISTEMP, Hansen *et al.*, 2010 and Lenssen *et al.* 2019).

2.1.1. Evaluation of ERA5 and CPC against IMD gridded observed data

Fig. 3 shows the trend in April maxima of the 4-day running mean of the daily maximum temperature (Tx4d) in the 1979-2023 period, for the three datasets selected for this study. The trends are lower in the ERA5 reanalysis product (Fig. 3(a)) than in CPC and IMD (Fig. 3(b-c)), with negative or zero trends in most parts of India, Bangladesh, Thailand and Lao PDR. The trends are consistent between the observation-based CPC and IMD datasets. The small differences between CPC and IMD are likely due to the difference in resolution (0.5° in CPC vs. 1° in IMD), which results in a smoother pattern in IMD. This consistency in trends between the CPC and IMD datasets is also demonstrated in higher temporal scales (see Fig. 3; Zachariah *et al.*, 2022). Notwithstanding the underestimation in trends, ERA5 is still able to capture the larger pockets with warming (and cooling) trends that are consistent with the other datasets.

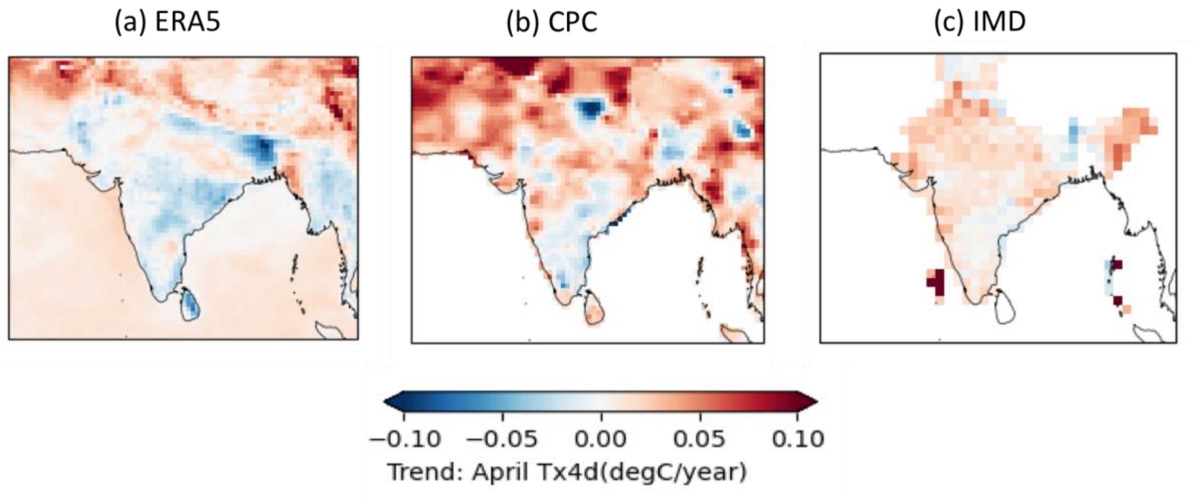

Figure 3: Trend in April maximum of 4-day running mean of daily maximum temperature (Tx4d) for 1979-2023, from (a) ERA5 (b) CPC and (c) IMD gridded products

Additionally, we compare the distribution of HIx4d over India from 17-20 April, 2023, calculated from ERA5 and IMD observed datasets. There is an overall agreement between ERA5 and IMD-based patterns both in terms of the HI (Fig. 1(a) vs. Fig. S2(a)) and the HI impact-based classifications (Fig. 1(c) vs. Fig. S2(b)). We note here that the IMD-based HI are calculated at 0.1°resolution (using inverse square distance weighted interpolation method) for daily timesteps on an experimental basis, from station-based 2m-dry bulb and 2m-dew point temperature. The change in near surface temperature due

to high terrain elevation is not incorporated in this interpolation technique at present (onging), and is therefore this data is only used for comparison against ERA5.
We also compare HIx4d at selected weather stations in six states in India that fall in the study domain (West Bengal, Andhra Pradesh, Tamil Nadu, Kerala, Goa and Maharashtra; Fig. S2(a)), with the ERA-5 based estimates from the nearest grid. The station-based estimates are available only for a short period (2006-2012) with gaps in the data at some locations. The ERA5-based estimates are found to perform reasonably well in all the selected locations, in terms of capturing the day-to-day variability (Fig. S2 (b)) and annual variability (Fig. S2(c)).

Therefore, we continue to use ERA5 for the analysis of HI, as this is the only product at hand that also has gridded daily dew point temperatures, which are required for calculating HI. However, as a consequence of the underestimated trends in Tx4d, the trends obtained from ERA5 for HIx4d are also likely a conservative estimate.

2.2 Model and experiment descriptions

We use two multi-model ensembles from climate modelling experiments using very different framings (Philip *et al.*, 2020): Coupled global circulation models (GCMs) and Sea Surface Temperature (SST) driven global circulation high-resolution models.

1. CMIP6. This consists of simulations from 17 GCMs with varying spatial resolutions. For more details on CMIP6, please see Eyring *et al.* (2016). The CMIP6 data that we use is based on historical simulations for the period 1850 to 2014, while the SSP2-4.5 scenario is used for the remainder of the 21st century.

2. HighResMIP SST-forced model ensemble (Haarsma *et al.*, 2016), the simulations for which span from 1950 to 2050. The SST and sea ice forcings for the period 1950-2014 are obtained from the 0.25° x 0.25° Hadley Centre Global Sea Ice and Sea Surface Temperature dataset that have undergone area-weighted regridding to match the climate model resolution.

2.3 Heat Index: background and computation

The Heat Index (HI) is calculated from a set of equations that use temperature and relative humidity as input. The HI equation was developed by Rothfusz (1990) by fitting a multiple regression model to pairs of temperature (in Fahrenheit) and relative humidity (in %) values that was previously calculated by Steadman (1979) from functional relationships that factor in the effects of these variables on human thermal comfort. The HI is equation is as follows:

$$\begin{aligned} HI \quad &= -42.379 + 2.04901523T + 10.14333127R - 0.22475541TR \\ &\quad -0.00683783T^2 - 0.05481717R^2 + 0.00122874T^2R \\ &\quad +0.00085282TR^2 - 0.00000199T^2R^2 \end{aligned} \tag{1}$$

where T is the daily maximum temperature in $°F$ and R is the relative humidity, expressed as a percentage from 0 to 100.

https://doi.org/10.25561/104092

The NOAA Weather Prediction Center uses a modified version of Eq (1) in their outlook, by making adjustments for extreme temperature and relative humidity conditions that are outside of the range of data considered by Steadman (1979) as follows:

$$HI = \begin{cases} HI - HI_{A1} & if\ R < 13\%\ and\ 80°F < T < 112°F \\ HI + HI_{A2} & if\ R > 85\%\ and\ 80°F < T < 87°F \\ HI & otherwise \end{cases} \quad (2)$$

where $HI_{A1} = [\frac{(13-R)}{4}]\sqrt{\frac{17-|T-95|}{17}}$ and $HI_{A2} = [\frac{(R-85)}{10}][\frac{87-T}{5}]$

If $HI < 80°F$ in Eq (2), then HI is recalculated as

$$HI = 0.5\,(T + 61 + 1.2(T - 68) + 0.094R). \quad (3)$$

T and HI in Eqs (1)-(3) are in Fahrenheit. As the remainder of the analysis is carried out in °C, HI is converted from °F to °C.

In this study, we use the NOAA Heat Index equations (Eqs (2) and (3)) to calculate the daily HI from the daily maximum temperature T and the relative humidity R. Where the relative humidity is not directly available, it is calculated as the ratio of the vapour pressure (e) to the saturation vapour pressure (e_s) from the daily mean dew point temperature ($Tdew$ in °C) and the daily maximum temperature ($Tmax$ in °C) , using the improved Magnus approximation proposed by Alduchov and Eskridge (1996):

$$R = 100 \times \frac{e}{e_s}, \quad (4)$$

where $e = exp\left(\frac{17.625\,Tdew}{243.04 + Tdew}\right)$ and $e_s = exp\left(\frac{17.625\,Tmax}{243.04 + Tmax}\right)$.

The data in model simulations (CMIP6 and HiResMip) are only available at daily resolution. Therefore, as in Schwingshackl *et al.* (2021), we assume that specific humidity is constant throughout the day and calculate the relative humidity from daily mean specific humidity and daily maximum temperature. HI is then calculated from the daily maximum temperature and the associated relative humidity using (1-3). For ERA5, Equation (4) was used assuming a constant dew point temperature throughout the day.

2.4 Statistical methods

In this analysis, we examine time series of April maxima of 4-day mean Heat Index (HIx4d), averaged for the IB and TL regions. Methods for observational and model analysis and for model evaluation and synthesis are used according to the World Weather Attribution Protocol, described in Philip *et al.* (2020), with supporting details found in van Oldenborgh *et al.* (2021), Ciavarella *et al.* (2021) and here.

https://doi.org/10.25561/104092

The analysis steps include: (i) trend calculation from observations; (ii) model validation; (iii) multi-method multi-model attribution and (iv) synthesis of the attribution statement.

To statistically model the event under study, we fit GEV distributions that shift with GMST to the HIx4d time series from the two regions to both the gridded observational datasets and the climate model output. We calculate the return periods, Probability Ratio (PR; the factor-change in the event's probability) and change in intensity of the event under study in order to compare the climate of now and the climate of the past, defined respectively by the GMST values of now and of the preindustrial past (1850-1900, based on the Global Warming Index). Next, results from observations and models that pass the validation tests are synthesised into a single attribution statement.

3 Observational analysis: return period and trend

3.1 Analysis of gridded data: Tx4d for IB and TL regions

The left panels in Fig 4 show the response of April Tx4d to GMST based on CPC (Fig. 4(a)) and ERA5 datasets (Fig. 4(c)) in the IB region. While the CPC dataset shows an increase in Tx4d with increasing GMST, the ERA5 dataset suggests that April maximum temperatures are becoming cooler under GMST in this region.

Fig. 4(b) shows GEV return period curves of Tx4d in the 2023 climate and in a counterfactual climate when the global mean temperature was cooler by 1.2°C for the CPC dataset. The 2023 Tx4d is estimated to be a 1-in-8 year event in the current climate, with uncertainty ranging from 4-35 years. The event is found to have been made 545 times more likely but with large uncertainties (uncertainty range: 0.34 - ∞) and 0.78ºC warmer (uncertainty: 0.4ºC cooler to 1.9ºC warmer) than in the 1.2° cooler climate. For the model attribution analysis we round the return period of the observed 2023 Tx4d over the IB region to 10 years.

We also tested whether the difference in these trends could be ascribed to the additional years covered by ERA5, by repeating the analysis using only records from 1979-2023. We find that the response of Tx4d to GMST continues to be decreasing (Fig. S4(a)). However, the trend is weaker in the shorter time series (-0.114°C per °C rise in GMST, compared to -0.435°C when using the full dataset). Using this shorter time series, the return period of the 2023 event in the current climate is approximately 1-in-10 years (Fig. S4(b)). Thus, due to inconsistencies in the ERA5 dataset in capturing the trends with time and the consistency of CPC with IMD over these regions, as shown in Fig. 3 in Section 2.1.1, we prefer the CPC-based return periods and fit parameters for evaluation of climate models and attribution analysis of Tx4d in the IB region.

https://doi.org/10.25561/104092

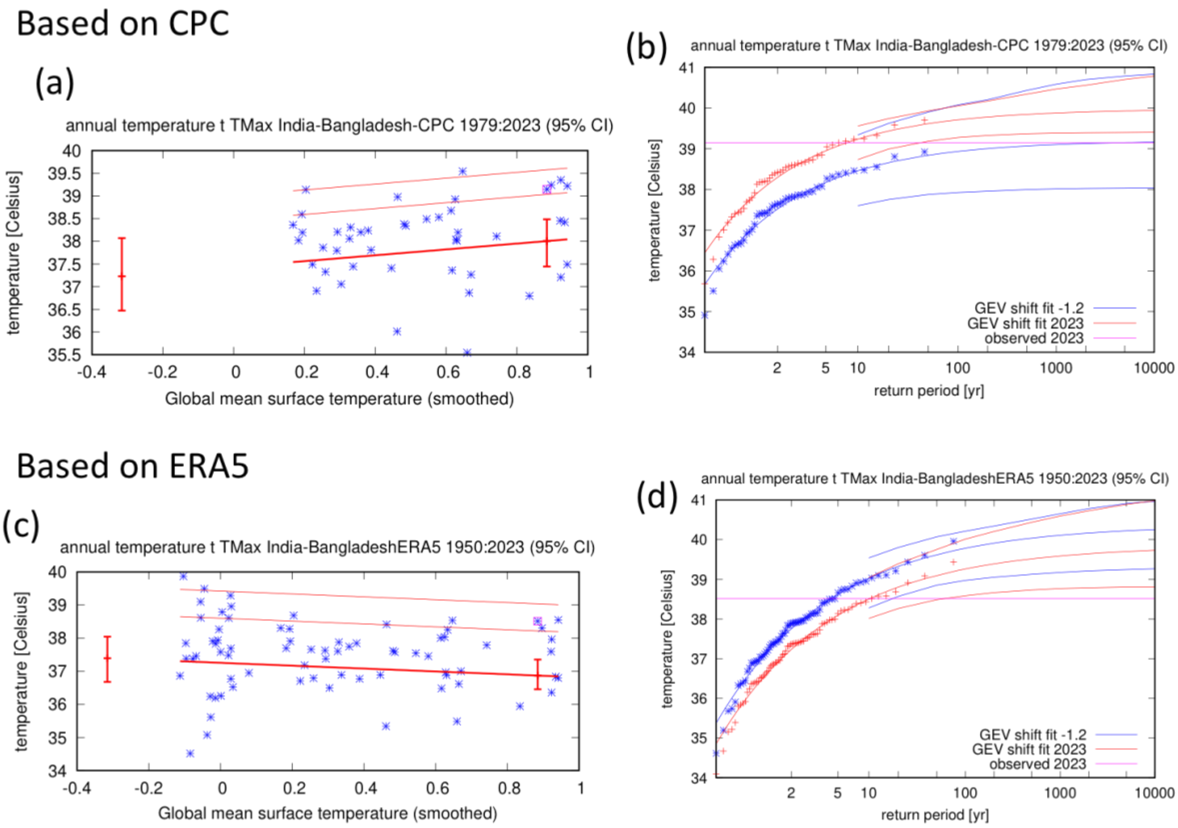

Figure. 4: (a) Regression of CPC April Tx4d over the IB region on global mean temperature. The thick red line denotes the location of the distribution, with the thinner red lines representing the 6-year (lower) and 40-year (upper) effective return levels. The vertical red lines show the 95% confidence interval for the location parameter, for the 2023 climate (right) and the hypothetical 1.2ºC cooler climate (left). The 2023 observation is highlighted with the magenta box. (b) Return periods for the 2023 climate (red lines) and the 1.2ºC cooler climate (blue lines with 95% CI), based on CPC data. (c) same as (a), but using ERA5 data. (d) same as (b), using ERA5 data.

The left panels in Fig 5 show the equivalent trends over the TL region for the CPC (Fig. 5(a)) and ERA5 datasets (Fig. 5(c)). Both datasets show increased April Tx4d in response to GMST, but the trend is smaller in ERA5, for reasons discussed in Section 2.2.1. It can be seen from the return period curves that unlike CPC where there is a clear climate change signal (Fig. 5(b)), the GMST signal is not discernible for ERA5 (Fig. 5(d)). Therefore, we continue the analysis for the TL region using CPC records.

The 2023 Tx4d is estimated to be a 1-in-13 year event in the current climate, with uncertainty ranging from 5-100 years. The event is found to have been made 5 times more likely but with large uncertainties (uncertainty range: 0.3 - ∞) and 0.79ºC warmer (uncertainty: 0.5ºC cooler to 2.1ºC warmer) than in the preindustrial climate. For the model attribution analysis we round the return period of the observed 2023 Tx4d over the TL region to 10 years.

https://doi.org/10.25561/104092

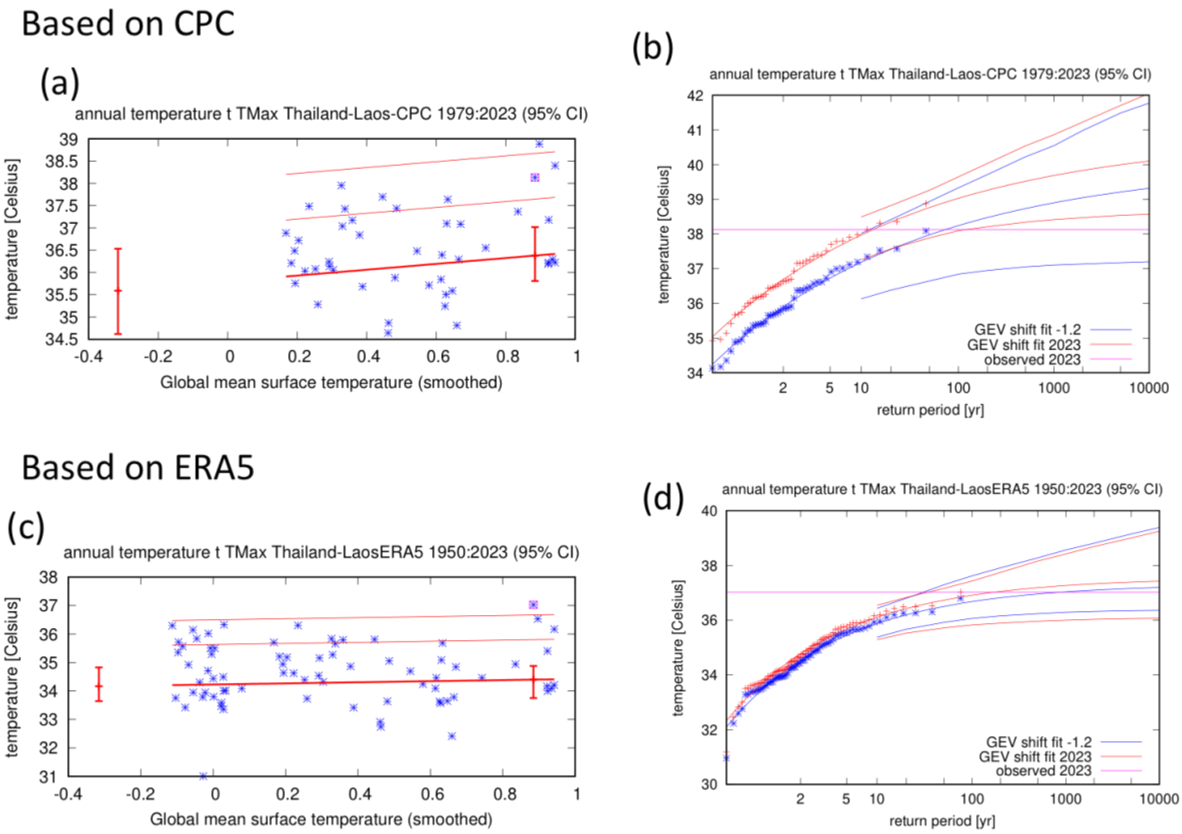

Figure 5**:** (a) Regression of CPC April Tx4d over the TL region on global mean temperature. The thick red line denotes the location of the distribution, with the thinner red lines representing the 6-year (lower) and 40-year (upper) effective return levels. The vertical red lines show the 95% confidence interval for the location parameter for the 2023 climate (right) and the hypothetical 1.2ºC cooler climate (left). The 2023 observation is highlighted with the magenta box. (b) Return periods for the 2023 climate (red lines) and the 1.2ºC cooler climate (blue lines with 95% CI), based on CPC data. (c) same as (a), but using ERA5 data. (d) same as (b), using ERA5 data.

3.2 Analysis of gridded data - Heat Index in IB region

Fig. 6 shows the time series of April *HIx4d*, averaged over the IB region, from ERA5. There is a consistent increase in HI from 1950 to 2023, with roughly 1ºC increase in HI between the first and the last decade of the series. Note that these values are averages over a large region, and local values are sometimes higher, nearing the “extreme danger” range: ERA5-calculated HI reached for instance 48°C in Dhaka, Bangladesh and exceeded 50°C in Kolkata, India during April 2023.

https://doi.org/10.25561/104092

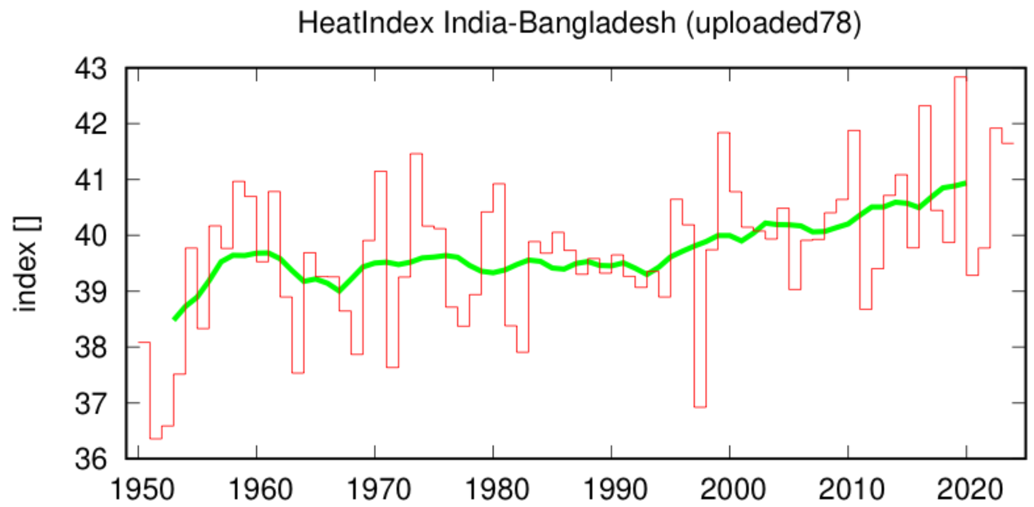

Figure 6: Time series of April HIx4d over IB region in ERA5, along with the ten-year running mean (green line).

Fig. 7(a) shows the IB HIx4d as a function of the global mean temperature, based on ERA5. As might be expected for a temperature-based index, HIx4d increases as the GMST increases. Fig. 7(b) shows GEV return period curves in the 2023 climate and a past climate when the global mean temperature was cooler by 1.2°C. The 2023 HIx4d is estimated to be a 1-in-5 year event in the 2023 climate, with uncertainty ranging from 2-12 years. The event is found to have been made at least 26 times more likely (best estimate: 400,000) and 2ºC warmer (uncertainty: 1.13 -3ºC) than in the 1.2° cooler climate. This may be conservative due to the underestimation of the trend in Tx4d in ERA5. For the model attribution analysis we define the 2023 HIx4x over the IB region as a 1-in-5 year event.

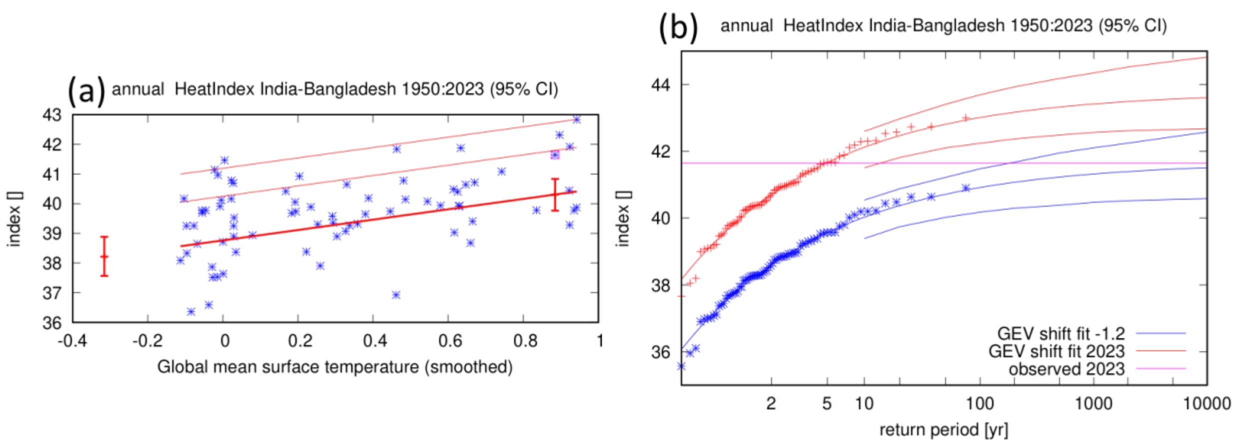

Figure 7: *(*a) Regression of April HIx4d (in °C) over the IB region on global mean temperature. The thick red line denotes the location of the distribution, with the thinner red lines representing the 6-year (lower) and 40-year (upper) effective return levels. The vertical red lines show the 95% confidence interval for the location parameter for the 2023 climate (right) and the hypothetical 1.2ºC cooler climate (left). The 2023 observation is highlighted with the magenta box. (b) Return period curves for the 2023 climate (red lines) and the 1.2ºC cooler climate (blue lines with 95% CI). The HIx4d is computed from ERA5 data.

https://doi.org/10.25561/104092

3.2 Analysis of gridded data - Heat Index in TL region

As with the IB region, an increasing trend in HIx4d is observed for the TL region (Fig. 8). The trends are slightly steeper in this region, with an increase of nearly 2°C in the HI between the first and last decades. Locally, ERA5-calculated HI reached the April record value of 48°C in the vicinity of both Vientiane and Bangkok, the capitals of the two countries.

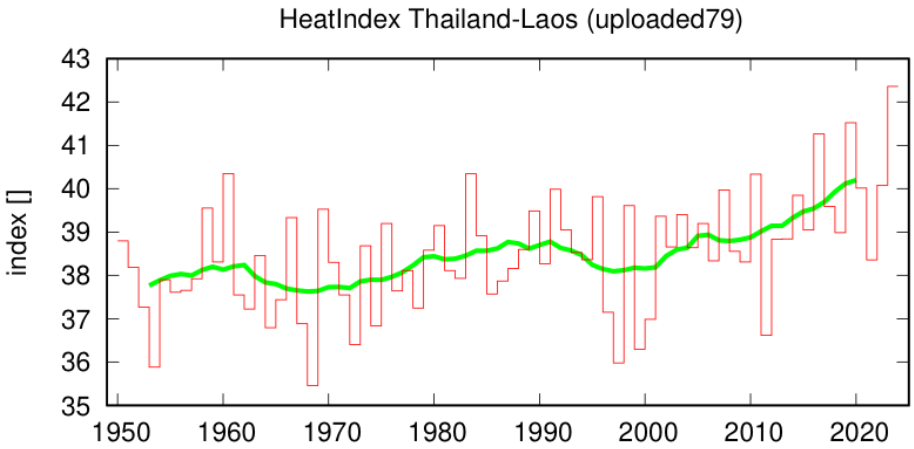

Figure 8: Time series of April HIx4d area-averaged over TL region, along with the ten-year running mean (shown by the green line) based on the ERA5 datasets.

There is also a strong sensitivity of the TL April HIx4d to the global mean temperature (Fig. 9(a)). In the GEV return period curves in Fig. 9(b), the 2023 observed April HIx4d over the TL region is seen to be a rare 1-in-200 year event even in the present climate (uncertainty: 37 years to ∞). The event is found to have been made at least 5400 times more likely (best estimate tends to ∞) and 2.4ºC warmer (uncertainty: 1.3 - 3.4ºC). These figures may be conservative due to the underestimation of the trend in Tx4d in ERA5. For the attribution analysis with climate models we define the 2023 HIx4d over the TL region as a 1-in-200 year event.

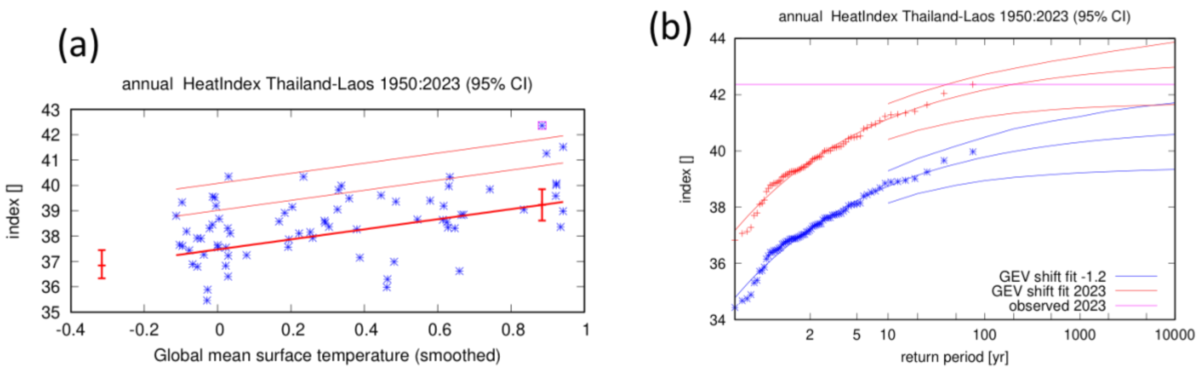

Figure 9: (a) Regression of April HIx4d (in degC), area-averaged over the TL region on global mean temperature. The thick red line denotes the location of the distribution, with the thinner red lines representing the 6-year (lower) and 40-year (upper) effective return levels. The vertical red lines show the 95% confidence interval for the location parameter in the 2023 climate (right) and the hypothetical 1.2ºC cooler climate (left). The 2023 observation is highlighted with the magenta box. (b) Return period curves for the 2023 climate (red lines) and the 1.2ºC cooler climate (blue lines with 95% CI). The HIx4d is computed from ERA5 data.

https://doi.org/10.25561/104092

4 Model evaluation

In the subsections below we show the results of the model evaluation for Heat Index, for the IB (Table 1) and the TL regions (Table 2). The evaluation period considered is 1950-2023, the length for which ERA5 observations are available. Model evaluation results for daily maximum temperature for the IB and TL regions against CPC records (1979-2023) are shown in Tables S1-S2. If five models or fewer perform well for a particular model setup, we include models that only just pass the validation tests for that model setup. The climate models are evaluated against the observations in their ability to capture:

1. Seasonal cycles: For this, we qualitatively compare the seasonal cycle of daily maximum temperatures and heat index in the climate model outputs against observation-based plots. We discard any models that exhibit multi-modality and/or ill-defined peaks in their seasonal cycles.

2. Spatial patterns: Models that do not match the observations in terms of the large-scale pattern of daily maximum temperatures and heat index during April are excluded.

3. Parameters of the fitted GEV model. We discard the model if the ranges of the shape and scale parameters do not overlap with those of the gridded observations.

The models are labelled as 'good', 'reasonable', or 'bad' based on their performances in terms of the three criteria discussed above. Finally, if the model is 'good' for all of these criteria, we give it an overall rating of 'good' (green highlight). We rate the model as 'reasonable' or 'bad', if it is rated 'reasonable' or 'bad', respectively, for at least one of the three criteria. These are respectively shown by the yellow and red highlights in the tables below.

Table 1: Evaluation results of the climate models considered for attribution analysis of the April 4-day maximum HI over the IB region. The table consists of qualitative assessments of the seasonal cycles and spatial patterns, the sigma and shape parameters from fitting a GEV distribution that shifts with GMST, and the effective return level of a 1-in-5 year event in the 2023 climate.

Observations	**Seasonal cycle**	**Spatial pattern**	**Sigma**	**Shape parameter**	**Event magnitude [°C]**
ERA5			1.14 (0.908 ... 1.31)	-0.33 (-0.46 ... -0.17)	41.65
Model					**Threshold for 5-year return period[°C]**
CMIP6					
ACCESS-CM2_r1i1p1f1.hssp245	good	good	0.710 (0.590 ... 0.800)	-0.22 (-0.38 ... -0.090)	40.54

https://doi.org/10.25561/104092

ACCESS-ESM1-5_r1i1p1f1.hssp245	good	good	0.970 (0.760 ... 1.15)	-0.41 (-0.67 ... -0.24)	41.59
CanESM5_r1i1p1f1.hssp245	reasonable	good	1.03 (0.820 ... 1.21)	-0.28 (-0.58 ... -0.18)	45.77
EC-Earth3_r1i1p1f1.hssp245	good	good	0.770 (0.650 ... 0.890)	-0.47 (-0.68 ... -0.39)	40.38
EC-Earth3-Veg_r1i1p1f1.hssp245	good	good	1.01 (0.740 ... 1.26)	-0.40 (-0.65 ... -0.21)	40.21
FGOALS-g3_r1i1p1f1.hssp245	good	good	0.760 (0.640 ... 0.860)	-0.30 (-0.48 ... -0.17)	39.95
GFDL-CM4_r1i1p1f1.hssp245	good	good	1.14 (0.890 ... 1.36)	-0.32 (-0.51 ... -0.13)	40.8
GFDL-ESM4_r1i1p1f1.hssp245	good	good	1.09 (0.860 ... 1.28)	-0.24 (-0.38 ... -0.070)	39.63
INM-CM4-8_r1i1p1f1.hssp245	good	good	1.02 (0.780 ... 1.20)	-0.37 (-0.58 ... -0.22)	38.86
INM-CM5-0_r1i1p1f1.hssp245	good	good	0.770 (0.550 ... 0.970)	-0.34 (-0.74 ... -0.090)	39.62
KACE-1-0-G_r1i1p1f1	good	good	0.520 (0.420 ... 0.610)	-0.24 (-0.39 … -0.09)	43.33
KIOST-ESM_r1i1p1f1.hssp245	bad	bad	1.03 (0.810 ... 1.22)	-0.33 (-0.51 ... -0.18)	49.64
MPI-ESM1-2-LR_r1i1p1f1.hssp245	good	good	1.05 (0.870 ... 1.19)	-0.21 (-0.52 ... -0.060)	39.41
MPI-ESM1-2-HR_r1i1p1f1.hssp245	good	good	1.05 (0.770 ... 1.26)	-0.38 (-0.71 ... -0.22)	40.79
MRI-ESM2-0_r1i1p1f1.hssp245	good	good	1.06 (0.860 ... 1.22)	-0.37 (-0.61 ... -0.20)	41.71
NorESM2-LM_r1i1p1f1.hssp245	good	good	0.950 (0.760 ... 1.09)	-0.18 (-0.42 ... 0.030)	39.07

https://doi.org/10.25561/104092

NorESM2-MM_r1i1p1f1.hssp245			1.03 (0.840 ... 1.22)	-0.35 (-0.56 ... -0.21)	40.22
HiResMIP					
HadGEM3-GC31-MM ()	good	good	0.990 (0.800 ... 1.17)	-0.42 (-0.63 ... -0.25)	42.54
MPI-ESM1-2-HR ()	good	good	1.50 (1.23 ... 1.74)	-0.42 (-0.64 ... -0.30)	41.05
CNRM-CM6-1-HR ()	good	good	1.17 (0.870 ... 1.38)	-0.29 (-0.46 ... -0.080)	40.37

Table 2: Evaluation results of the climate models considered for attribution analysis of the April 4-day maximum HI over the TL region. The table consists of qualitative assessments of the seasonal cycles and spatial patterns, the sigma and shape parameters from fitting a GEV distribution that shifts with GMST, and the effective return level of a 1-in-200 year event in the 2023 climate.

Observations	**Seasonal cycle**	**Spatial pattern**	**Sigma**	**Shape parameter**	**Event magnitude [°C]**
ERA5			1.14 (0.907 ... 1.32)	-0.28 (-0.43 ... -0.17)	
Model					**Threshold for 200-year return period[°C]**
CMIP6					
ACCESS-CM2_r1i1p1f1 ssp245 ()	good	good	0.740 (0.610 ... 0.850)	-0.31 (-0.53 ... -0.18)	40.25
ACCESS-ESM1-5_r1i1p1f1 ssp245 ()	good	good	0.850 (0.690 ... 0.970)	-0.18 (-0.32 ... -0.050)	46.72
CanESM5_r1i1p1f1 ssp245 ()	good	good	1.47 (1.21 ... 1.72)	-0.29 (-0.66 ... -0.080)	48.45
EC-Earth3_r1i1p1f1 ssp245 ()	good	good	1.23 (1.02 ... 1.42)	-0.30 (-0.61 ... -0.20)	41.82
EC-Earth3-Veg_r1i1p1f1 ssp245 ()	good	good	1.54 (1.23 ... 1.85)	-0.38 (-0.75 ... -0.25)	41.58

https://doi.org/10.25561/104092

FGOALS-g3_r1i1p1f1 ssp245 ()	good	good	0.920 (0.670 ... 1.09)	-0.45 (-0.70 ... -0.18)	41.86
GFDL-CM4_r1i1p1f1 ssp245 ()	good	good	1.45 (1.27 ... 1.49)	-0.63 (-0.76 ... -0.57)	42.94
GFDL-ESM4_r1i1p1f1 ssp245 ()	good	good	1.46 (1.20 ... 1.68)	-0.51 (-0.69 ... -0.33)	42.21
INM-CM4-8_r1i1p1f1 ssp245 ()	good	good	1.21 (0.920 ... 1.43)	-0.060 (-0.27 ... 0.13)	40.43
INM-CM5-0_r1i1p1f1 ssp245 ()	good	good	1.68 (1.38 ... 2.07)	-0.44 (-0.78 ... -0.26)	39.58
KACE-1-0-G_r1i1p1f1 ssp245 ()	good	good	0.710 (0.570 ... 0.840)	-0.32 (-0.54 ... -0.17)	44.82
KIOST-ESM_r1i1p1f1 ssp245 ()	bad	bad	1.10 (0.900 ... 1.29)	-0.23 (-0.43 ... -0.080)	53.1
MPI-ESM1-2-LR_r1i1p1f1 ssp245 ()	good	good	1.36 (1.02 ... 1.65)	-0.36 (-0.57 ... -0.13)	41.48
MPI-ESM1-2-HR_r1i1p1f1 ssp245 ()	good	good	1.04 (0.850 ... 1.20)	-0.22 (-0.38 ... -0.070)	43.59
MRI-ESM2-0_r1i1p1f1 ssp245 ()	good	good	1.47 (1.19 ... 1.78)	-0.29 (-0.72 ... -0.15)	44.69
NorESM2-LM_r1i1p1f1 ssp245 ()	good	good	0.830 (0.670 ... 0.990)	-0.20 (-0.39 ... 0.010)	41.13
NorESM2-MM_r1i1p1f1 ssp245 ()			1.09 (0.870 ... 1.28)	-0.29 (-0.45 ... -0.16)	42.18
HiResMIP					
HadGEM3-GC31-MM sst ()	good	good	0.830 (0.690 ... 0.950)	-0.39 (-0.58 ... -0.26)	43.4
MPI-ESM1-2-HR sst ()	good	good	1.72 (1.35 ... 2.05)	-0.55 (-0.79 ... -0.44)	41.6
CNRM-CM6-1-HR sst ()	good	good	1.11 (0.900 ... 1.28)	-0.13 (-0.34 ... 0.050)	41.8

5 Multi-method multi-model attribution

This section shows probability ratios (PR) and changes in intensity (ΔI) for models that passed validation, for analysing HIX4d in th IB (Table 3) and TL regions (Table 4). Similar tables for Tx4d (Tables S3-S4) are provided in the supplement.

https://doi.org/10.25561/104092

Table 3: Probability ratio and change in intensity of HIx4d in the IB region, for models that passed the validation tests for (a) past vs. present and (b) present vs. future.

Model / Observations	**a. Past vs. present**		**b. Present vs. future**	
	Probability ratio PR [-]	**Change in intensity ΔI [°C]**	**Probability ratio PR [-]**	**Change in intensity ΔI [°C]**
ERA5	4.3e+5 (26 ... ∞)	2.1 (1.1 ... 3.0)		
ACCESS-ESM1-5_r1i1p1f1.hssp245 ssp245 ()	25 (3.8 ... 1.0e+4)	0.96 (0.40 ... 1.6)	2.7 (2.3 ... 3.6)	0.87 (0.67 ... 1.1)
CanESM5_r1i1p1f1.hssp245 ssp245 ()	1.0e+4 (9.6e+2 ... 1.0e+4)	2.9 (2.3 ... 3.5)	3.9 (3.1 ... 6.2)	1.7 (1.6 ... 1.9)
GFDL-CM4_r1i1p1f1.hssp245 ssp245 ()	14 (2.4 ... 1.0e+4)	1.3 (0.44 ... 2.1)	2.8 (2.3 ... 3.7)	1.2 (0.89 ... 1.4)
GFDL-ESM4_r1i1p1f1.hssp245 ssp245 ()	4.8 (1.0 ... 43)	1.0 (0.020 ... 2.0)	2.6 (2.0 ... 3.3)	1.1 (0.69 ... 1.5)
INM-CM4-8_r1i1p1f1.hssp245 ssp245 ()	8.4 (0.73 ... 1.0e+4)	0.89 (-0.18 ... 2.2)	2.9 (2.2 ... 4.3)	0.97 (0.68 ... 1.3)
MPI-ESM1-2-LR_r1i1p1f1.hssp245 ssp245 ()	19 (4.4 ... 1.0e+4)	1.8 (0.90 ... 2.7)	2.2 (1.6 ... 3.2)	0.78 (0.42 ... 1.1)
MPI-ESM1-2-HR_r1i1p1f1.hssp245 ssp245 ()	4.2 (0.23 ... 1.0e+4)	0.69 (-0.52 ... 1.8)	2.1 (1.7 ... 2.8)	0.70 (0.43 ... 1.1)
MRI-ESM2-0_r1i1p1f1.hssp245 ssp245 ()	2.5 (0.36 ... 22)	0.50 (-0.50 ... 1.3)	2.8 (2.3 ... 3.7)	1.1 (0.78 ... 1.4)
NorESM2-LM_r1i1p1f1.hssp245 ssp245 ()	3.3 (0.73 ... 1.0e+4)	0.82 (-0.27 ... 2.0)	2.6 (2.0 ... 3.4)	0.94 (0.61 ... 1.3)
NorESM2-MM_r1i1p1f1.hssp245 ()	1.0e+4 (4.3e+3 ... 1.0e+4)	2.6 (1.9 ... 3.4)	3.7 (2.9 ... 5.3)	1.7 (1.3 ... 2.0)
HadGEM3-GC31-MM ()	1.0e+4 (1.0e+4 ... 1.0e+4)	2.1 (1.2 ... 2.9)	<not computed>	<not computed>
MPI-ESM1-2-HR ()	7.9e+2 (6.1 ... 1.0e+4)	1.8 (0.60 ... 3.0)	<not computed>	<not computed>
CNRM-CM6-1-HR ()	41 (6.3 ... 1.0e+4)	1.8 (0.82 ... 2.7)	<not computed>	<not computed>

Table 4: Probability ratio and change in intensity of HIx4d in the TL region, for models that passed the validation tests for (a) past vs. present and (b) present vs. future.

Model / Observations	**a. Past vs. present**		**b. Present vs. future**	
	Probability ratio PR [-]	**Change in intensity ΔI [°C]**	**Probability ratio PR [-]**	**Change in intensity ΔI [°C]**
ERA5	∞ (5.4e+3 ... ∞)	2.4 (1.3 ... 3.4)		
ACCESS-ESM1-5_r1i1p1f1 ssp245 ()	7.4e+3 (9.3 ... 1.0e+4)	1.5 (0.91 ... 2.1)	10 (3.6 ... 4.8e+2)	1.0 (0.80 ... 1.2)
CanESM5_r1i1p1f1 ssp245 ()	1.0e+4 (40 ... 1.0e+4)	3.2 (2.5 ... 3.9)	30 (0.00010 ... 1.0e+4)	1.9 (1.7 ... 2.1)
EC-Earth3_r1i1p1f1 ssp245 ()	1.0e+4 (1.9e+3 ... 1.0e+4)	2.0 (1.5 ... 2.5)	21 (0.00010 ... 2.0e+2)	1.1 (0.86 ... 1.4)

https://doi.org/10.25561/104092

EC-Earth3-Veg_r1i1p1f1 ssp245 ()	1.0e+4 (1.0e+4 ... 1.0e+4)	1.9 (0.60 ... 2.7)	23 (0.00010 ... 9.1e+2)	1.2 (0.86 ... 1.5)
FGOALS-g3_r1i1p1f1 ssp245 ()	1.0e+4 (1.0e+4 ... 1.0e+4)	1.4 (0.68 ... 2.2)	63 (0.00010 ... 9.1e+2)	1.3 (0.96 ... 1.5)
GFDL-CM4_r1i1p1f1 ssp245 ()	1.0e+4 (7.5 ... 1.0e+4)	2.7 (2.2 ... 2.9)	77 (0.00010 ... 9.1e+2)	1.5 (1.3 ... 1.6)
GFDL-ESM4_r1i1p1f1 ssp245 ()	1.0e+4 (1.0e+4 ... 1.0e+4)	2.2 (0.77 ... 2.9)	50 (0.00010 ... 1.0e+4)	1.5 (1.1 ... 1.9)
INM-CM4-8_r1i1p1f1 ssp245 ()	21 (3.0 ... 1.0e+4)	2.4 (0.90 ... 3.6)	4.2 (2.3 ... 52)	1.4 (1.0 ... 1.7)
MPI-ESM1-2-LR_r1i1p1f1 ssp245 ()	1.0e+4 (20 ... 1.0e+4)	1.7 (0.46 ... 2.8)	15 (0.00010 ... 9.1e+2)	0.99 (0.63 ... 1.4)
MPI-ESM1-2-HR_r1i1p1f1 ssp245 ()	1.0e+4 (5.4 ... 1.0e+4)	1.6 (0.55 ... 2.6)	8.7 (0.00010 ... 9.1e+2)	0.74 (0.36 ... 1.2)
MRI-ESM2-0_r1i1p1f1 ssp245 ()	1.0e+4 (7.0 ... 1.0e+4)	1.7 (-0.18 ... 2.8)	16 (0.00010 ... 4.8e+2)	1.5 (1.1 ... 1.9)
NorESM2-LM_r1i1p1f1 ssp245 ()	1.0e+4 (11 ... 1.0e+4)	2.2 (1.4 ... 3.1)	63 (0.00010 ... 1.0e+4)	1.6 (1.3 ... 1.9)
NorESM2-MM_r1i1p1f1 ssp245 ()	1.0e+4 (1.5e+3 ... 1.0e+4)	2.8 (1.8 ... 3.8)	53 (0.00010 ... 1.0e+4)	1.7 (1.4 ... 2.0)
HadGEM3-GC31-MM sst ()	1.0e+4 (1.0e+4 ... 1.0e+4)	2.5 (1.8 ... 3.1)	<not computed>	<not computed>
CNRM-CM6-1-HR sst ()	1.4e+3 (4.5 ... 1.0e+4)	2.5 (1.6 ... 3.4)	<not computed>	<not computed>

6 Hazard synthesis

For the event definitions described above we evaluate the influence of anthropogenic climate change on the events by calculating the probability ratio and change in intensity using observations and climate models. Models which do not pass the validation tests described in section 4 are excluded from the analysis. The aim is to synthesise results from models that pass the evaluation along with the observation-based products, to give an overarching attribution statement. Figures 10 to 17 show the changes in probability and intensity for the observations (blue) and models (red). To combine them into a synthesised assessment, first, for the analyses in which two observational series have been used, a representation error is added (in quadrature) to the observations, to account for the difference between observations-based datasets that cannot be explained by natural variability. This is shown in these figures as white boxes around the light blue bars. The dark blue bar shows the average over the observation-based products. Next, a term to account for intermodel spread is added (in quadrature) to the natural variability of the models. This is shown in the figures as white boxes around the light red bars. The dark red bar shows the model average, consisting of a weighted mean using the (uncorrelated) uncertainties due to natural variability plus the term representing intermodel spread (i.e., the inverse square of the white bars). Observation-based products and models are combined into a single result in two ways. Firstly, we neglect common model uncertainties beyond the intermodel spread that is depicted by the model average, and compute the weighted average of models (dark red bar) and observations (dark blue bar): this is indicated by the magenta bar. Because, due to common model uncertainties, model uncertainty can be larger than the intermodel spread, we also show the more conservative estimate of an unweighted, direct average of observations (dark red bar) and models (dark blue bar) contributing 50% each, indicated by the white box around the magenta bar in the synthesis figures. Because results from observations and models correspond quite well to each other, in this study we use the weighted average (magenta bar).

Figures 10-11 show the results of this assessment, for Hix4d in the IB and TL regions respectively.

https://doi.org/10.25561/104092

Individual models show a range of different results, with all of them suggesting an increase in likelihood of this variable due to climate change (Fig. 10(a) and Fig. 11(a)). For the IB region, our synthesis gives a probability ratio of at least 30 (best estimate: 3300) and a corresponding change in intensity of 1.9°C (1.13°C - 2.65°C). For the TL region, the observed Hix4d would have been virtually impossible without climate change (lower bound: 5430), and 2.2°C cooler.

For the changes in intensity and likelihood under further warming we compare the model simulations for a 2°C warmer world with those of today's climate using the same synthesis methods described above. The change in probability for a further 0.8°C global temperature increase is PR= 3 (2-4) for the IB region (Fig. 12(a)) with an additional increase in intensity of 1°C (0.5°C - 1.7°C; Fig. 12(b)). Over the TL region, the event is expected to become 8 times more likely at 2°C global warming levels- PR = 8 (uncertainty: 3-41; Fig. 13(a)), with an additional increase in intensity of 1.3°C (0.8°C -2°C; Fig. 13(b)).

We note here that this analysis used an index which spatially averages the values of the heat index over large regions. In both regions the average index is about 42°C in 2023. It is important to consider that this average index has a significant spatial variability, with values in some locations reaching in the upper range of temperatures found as "dangerous" and in some places nearing the "extremely dangerous" range. Therefore, under 2°C global climate change, when the average HI in each region is expected to increase by a further 1°C, the probability of exceeding the "extremely dangerous" threshold locally will also increase significantly, in particular in urban areas where the heat island effect plays an important role.

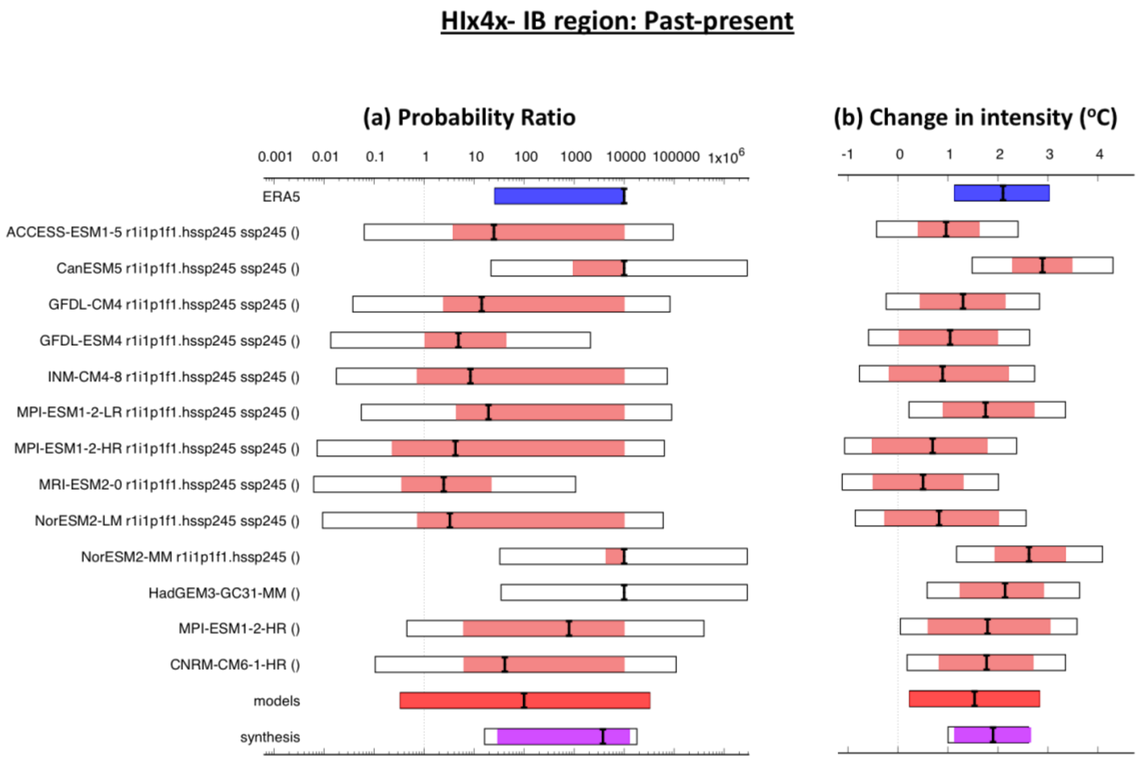

Figure 10: Synthesis of (a) probability ratios and (b) intensity changes when comparing the return period and magnitudes of the 4-day average HI over the IB region in the current climate and a 1.2ºC cooler climate.

https://doi.org/10.25561/104092

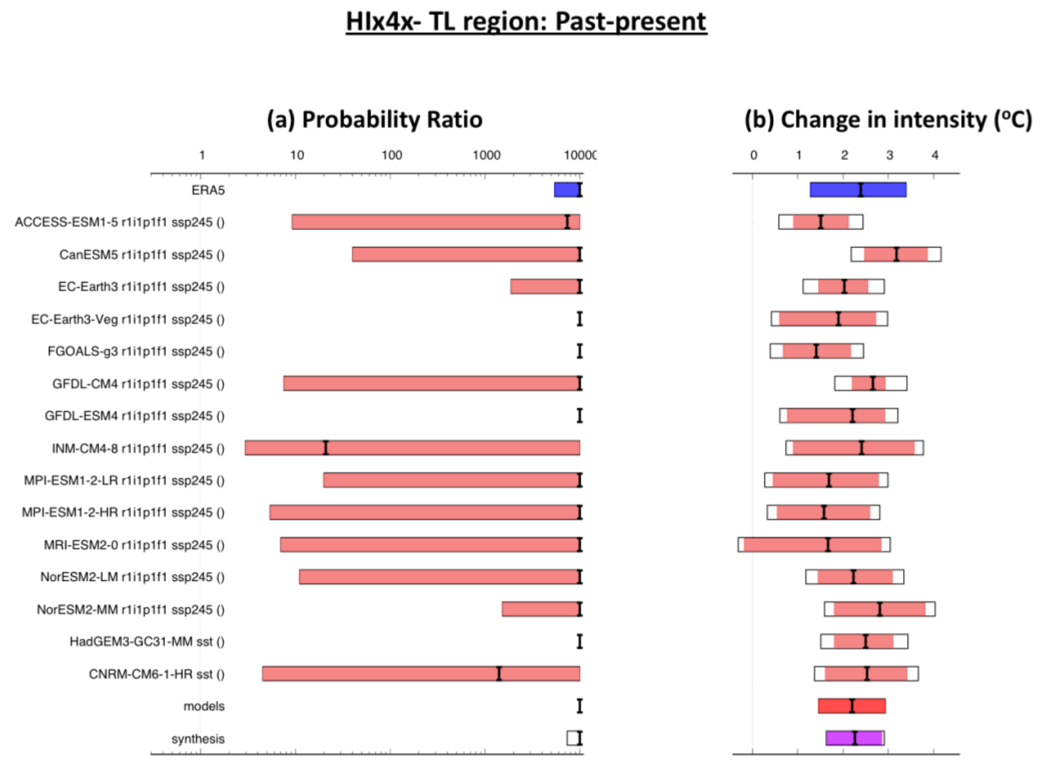

Figure 11: Synthesis of (a) probability ratios and (b) intensity changes when comparing the return period and magnitudes of the 4-day average HI over the TL region in the current climate and a 1.2°C cooler climate.

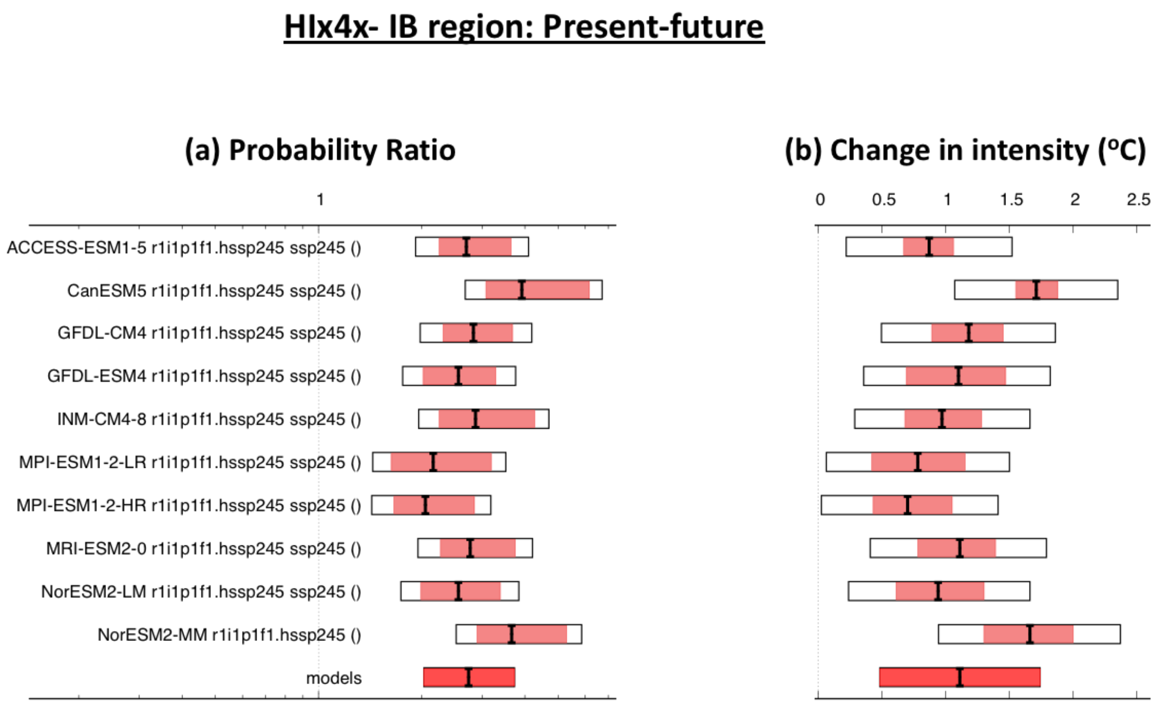

Figure 12: Synthesis of (a) probability ratios and (b) intensity changes when comparing the return period and magnitudes of the 4-day average HI over the IB region in the current climate and a 2°C warmed climate.

https://doi.org/10.25561/104092

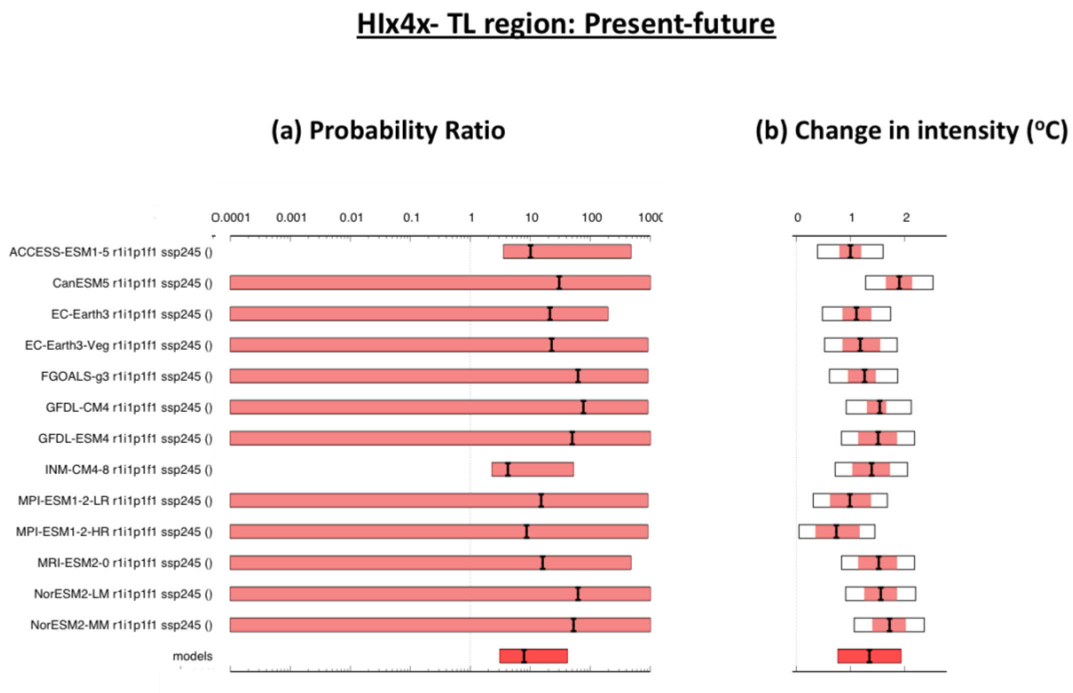

Figure 13: Synthesis of (a) probability ratios and (b) intensity changes when comparing the return period and magnitudes of the 4-day average HI over the TL region in the current climate and a 2°C warmed climate.

We additionally examine the role of climate change in the April Tx4d in these regions (Figs. 14-15). There is an overall agreement between the observations and models in that the climate change signal is found to be positive in both regions. The event is found to have been made about 40 times more likely (uncertainty: 0.2-8220) and 0.6°C (uncertainty: -0.18°C to 1.4°C) more intense by climate change in the IB region (Fig. 14). For the TL region (Fig. 15), the is PR=27 (0.8-3300) with an increase in temperature of 1°C (0.5°C to 1.7°C).
For the IB region, where observed records are available from IMD and where the trends in ERA5 were found to be underestimated (see Section 2.1.1), we also analyse the sensitivity of results to the exclusion of ERA5 (not shown). With only CPC representing the observational trend, the observed trend and change in intensity are larger than when ERA5 was included. This difference also propagates into the overall values from combining the observations and models, and the synthesis indicates slightly larger changes that do no longer encompass no change. Therefore, the estimates for HIx4d may also be conservative.

The change in probability from now to 2°C warming levels suggest an expected doubling of likelihood in both regions (Fig. 16(a) and Fig. 17(a)) with an expected increase in temperature of 0.5degC in the IB region (Fig. 16(b)) and 0.7°C in the TL region (Fig. 17(b)).

https://doi.org/10.25561/104092

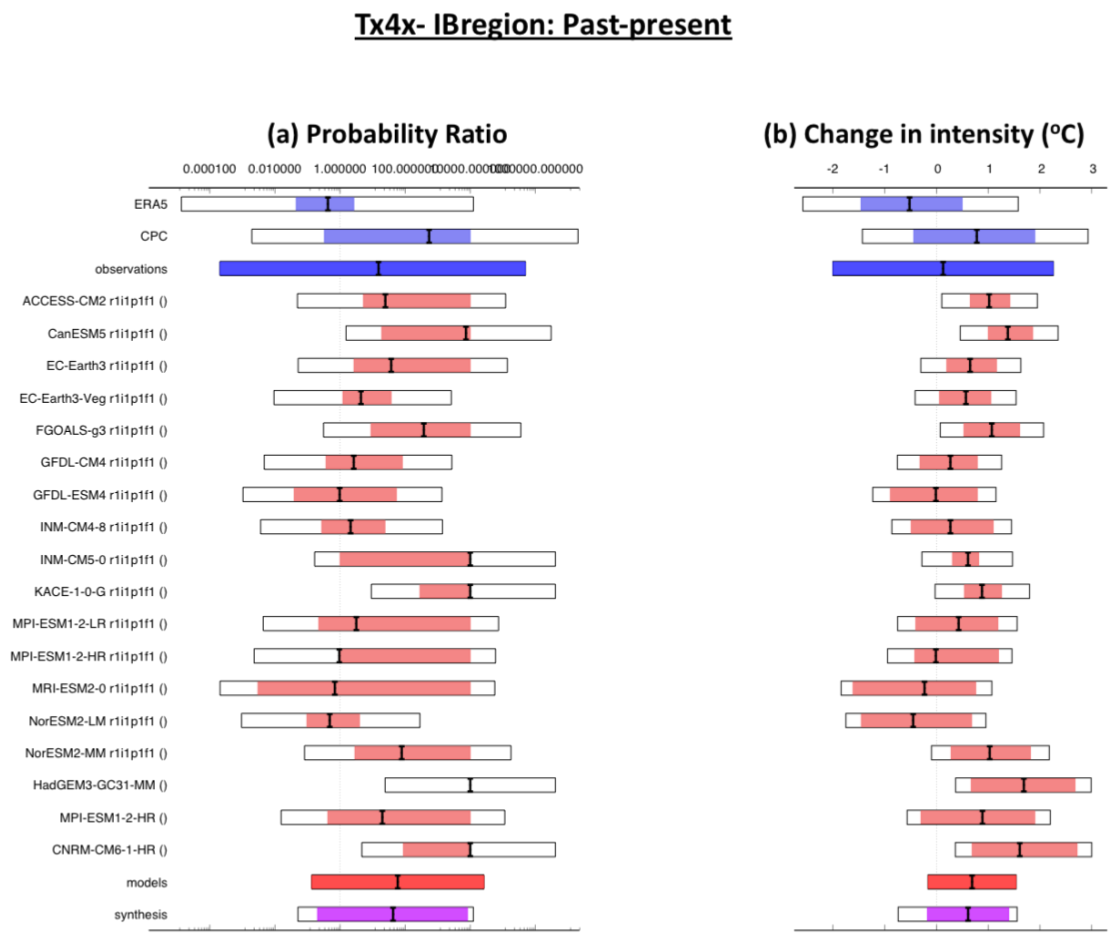

Figure 14: Synthesis of (a) probability ratios and (b) intensity changes when comparing the return period and magnitudes of the 4-day average maximum temperature over the IB region in the current climate and a 1.2ºC cooler climate.

https://doi.org/10.25561/104092

Tx4x- TLregion: Past-present

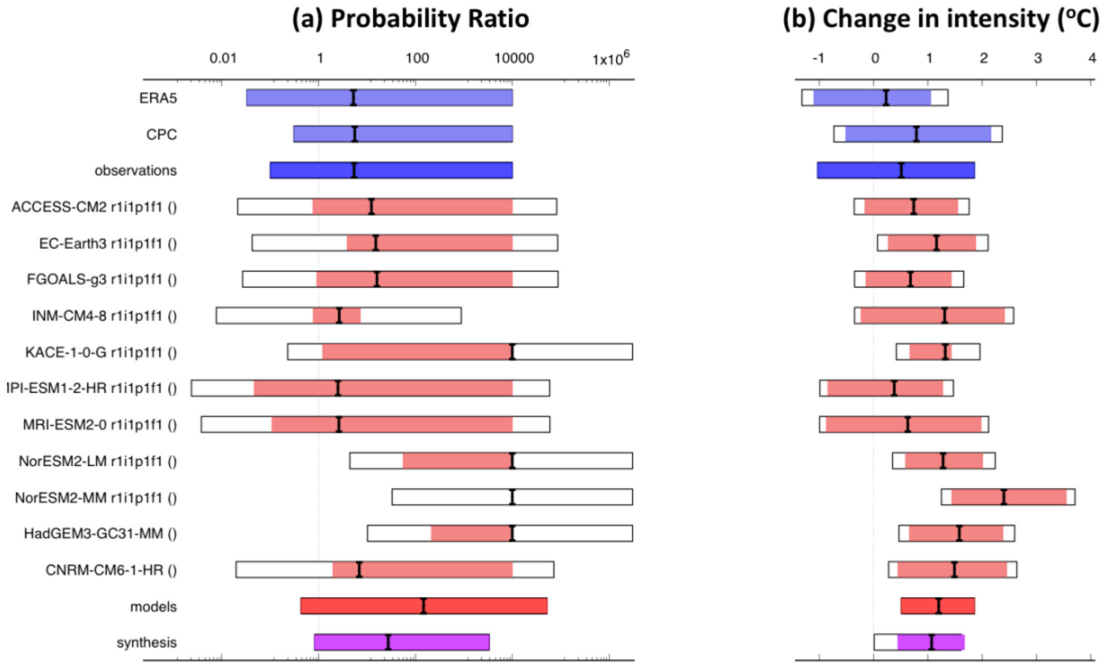

Figure 15: Synthesis of (a) probability ratios and (b) intensity changes when comparing the return period and magnitudes of the 4-day average maximum temperature over the TL region in the current climate and a 1.2°C cooler climate.

Tx4x- IBregion: Present-future

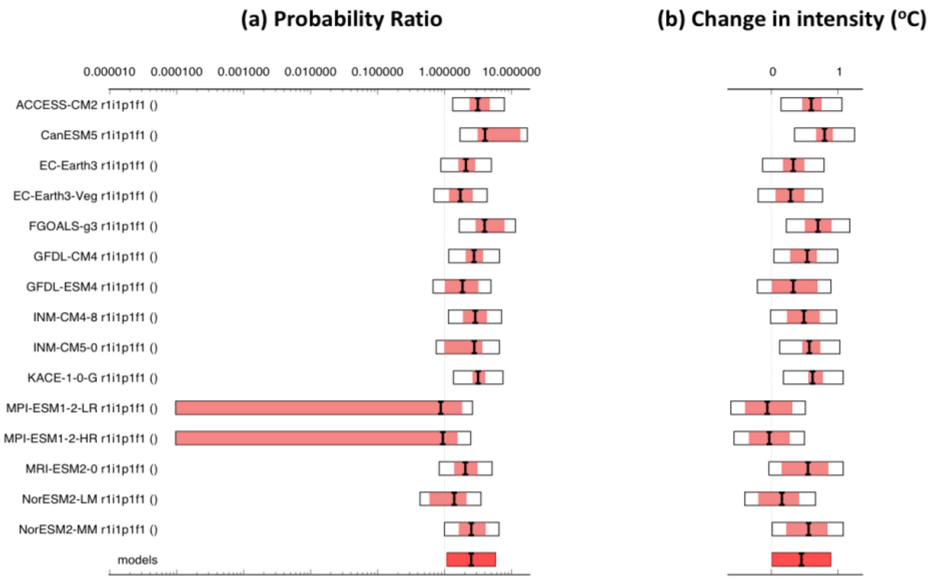

Figure 16: Synthesis of (a) probability ratios and (b) intensity changes when comparing the return period and magnitudes of the 4-day average maximum temperature over the IB region in the current climate and a 2°C warmed climate.

https://doi.org/10.25561/104092

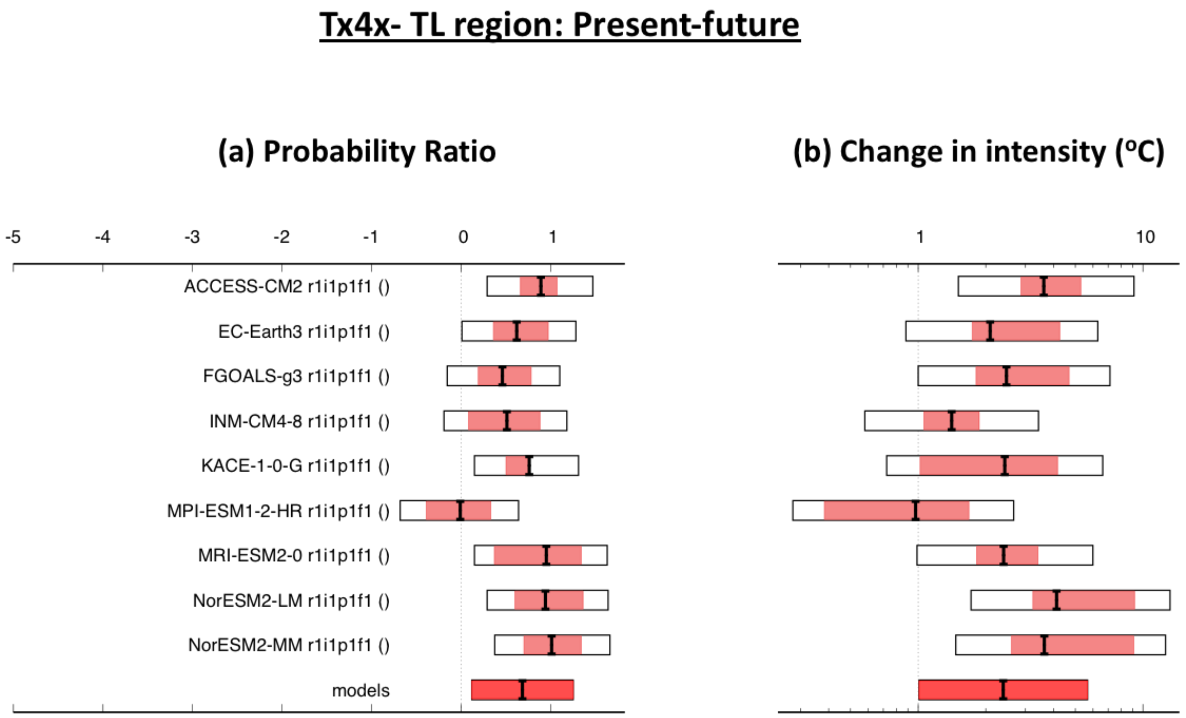

Figure 17: Synthesis of (a) probability ratios and (b) intensity changes when comparing the return period and magnitudes of the 4-day average maximum temperature over the TL region in the current climate and a 2°C warmed climate.

7 Vulnerability and exposure

Vulnerability and exposure are central to understanding disaster impacts, and include various socio-political and economic factors. The impacts of heatwaves on health across South Asia have been extensively studied in scoping reviews by Dimitrova *et al.* (2020) and Tiwari *et al.* (2022), and they indicate that a heatwave day has about 20% higher mortality risk than a non-heatwave day. In general, extreme heat risk stems from physiological vulnerabilities, high exposure to heat, and systemic inequities that reduce or limit access to services, information, economic opportunity, and basic needs (e.g. food and water). In individuals, many of these factors often intersect, and compound on one another.

7.1 Intersecting vulnerabilities

People vulnerable in situations of extreme heat typically include the elderly, those with pre-existing medical conditions such as cardiovascular disease or diabetes, pregnant and breastfeeding women, those taking certain medications, and those with mental health considerations. Those working in outdoor occupations such as construction, farming and street vending are also at heightened risk (Singh *et al.*, 2019).

Inequality and societal discrimination can also make it exceedingly difficult for vulnerable groups to undertake protective measures. Such systemic and coupled drivers of discrimination include: gender, race, ethnicity, caste, religion, age, disability, economic status, migrant status, and more, and are well

https://doi.org/10.25561/104092

documented in India (Himanshu, 2019). For example, Nomadic and Denotified Tribes are frequently overlooked in development schemes and subjected to exploitation, harassment, and legal injustices and also experience high structural vulnerability, as documented for the Indian cities of Kochi, Surat, and Mumbai (Santha *et al.*, 2016). Very few have access to affordable and effective health care services, government doctors, or urban health care providers – for them, waiting long hours at public hospitals or seeking private doctors is out of reach. This lack of access to health care can become fatal (Campbell *et al.*, 2018).

7.1.1 Gender-related heat risk

Socio-cultural and socio-political discrimination tied to gendered norms and practices is another major driver of heat-related suffering and harm, while reducing gender inequities can contribute to climate-resilient development (Andrijevic *et al.*, 2023). Analogue to the lived experiences of girls and women during cyclones, societal expectations in Bangladesh dictate that women stay put, indoors, and care for children and elderly household members, typically covering their hair and skin (the practice of *purdah*), all of which heighten their own risks of experiencing harm while delaying evacuation efforts (Chowdhury *et al.*, 2022; Ferdous and Mallick, 2019).

One study found that, in a Kolkata slum, there was little gender difference in heat stress experiences, yet in rural Parganas, elderly women suffered more heat stress than men because of childcare and household tasks like cooking and getting water (about 50-200m away from houses) (Mukhopadhyay and Weitz, 2022). Another study shows that elderly women in Parganas were significantly more likely to report nausea/vomiting, muscle cramps, disturbed sleep, prickly heat, and dizziness than elderly men due to a lower capacity to sweat and release heat. This could be due to lower fitness levels and higher body fat percentages (Mukhopadhyay and Weitz, 2022). The rural female heat experience was also confirmed in Tiwari *et al.* (2022)'s review, which suggested that women tend to bear greater heat impact than men because of existing gender inequality, cultural norms, roles and decision-making practices, while at the same time receiving fewer resources and less food.

7.1.2 Occupational heat risk

Many heat risks come about due to the occupations that expose workers to extremely hot and humid conditions. It is often the most marginalised members of society who end up in these positions. For example, migrants, having left rural regions in search of work in urban centres, are among the most marginalised people in India. They often lack local citizenship rights, political patronage, and social safety nets while facing unsafe housing conditions on top of ethnic, caste, gender, and/or religious prejudice and patterns of exclusion (Chu and Michael, 2019; Lundgren-Kownacki *et al.*, 2018; Santha *et al.*, 2016).

Another example are waste pickers, such as those in Bengaluru and many other cities in India, who work long hours in extreme temperatures, face social stigmatisation, have to seek water from expensive tankers, and are repeatedly left out of disaster risk consultations or, at best, constitute a tick box in participatory heat action planning (Chu and Michael, 2019).

Migrant brick kiln workers, frequently involving whole families with children, are doubly exposed to extreme outdoor temperature (40-45°C) and radiant heat from the furnaces (up to 52°C), such as those near Chennai, yet lack access to clean drinking water and sanitation (Lundgren-Kownacki *et al.*, 2018). They are also unlikely to afford transportation to get themselves to cool refugees such as movie theatres or malls.

Agricultural labourers are exposed to extreme temperatures and are directly affected by worsening air pollution. Agriculture is a primary industry and contributes heavily to the GDP and is the biggest employer in Lao People's Democratic Republic (PDR) (ADB, 2021a) and Thailand (ADB, 2021b). Heat stress also has negative impacts on livestock, which can in turn impact farmers' income (Thorntorn *et al.*, 2021).

A study by Venygopal *et al.* (2021) compares heat stress among indoor and outdoor workers. It was concluded that those working outdoors (farmers) had higher core body temperature, and were 2-3 times more at risk of dehydration, changes in urine volume and colour, and hence a higher chance of reduced kidney function compared to those working indoors (e.g. steelworkers). Overall, there is a 10-fold higher chance of productivity loss among outdoor workers in times of heat stress. Indoor workers, on the other hand, tended to have mechanisation/automation that reduces work intensity and had better welfare facilities and cooling equipment, including in labour intensive industries.

A comparison study of heat stress in the elderly (over 60) between two contrasting settings - Kolkata slums (iron workers, shopkeepers, housemaids, labourers) and Parganas district in West Bengal (rice farmers) - revealed significant importance. Weitz *et al.* (2022) show that, in general, the elderly who remain active in their occupation experienced about 2-3°C higher temperatures than those inactive residents. Between the two sites, elderly Kolkata slum dwellers were 4 times more likely to experience dangerous heat index levels of over 45°C for longer hours compared to rural village elderly. This is primarily because they had no air conditioner, the house construction material absorbs heat, and because of the urban heat island effect in slums; all combined to create hotter indoor conditions, especially during the night time. In the slums, people also shut their doors due to security reasons while many houses lacked windows, thus air ventilation was minimal.

7.1.3 Age-related heat risk

Older adults (>60yrs) typically experience a decline in cardiovascular systems which heightens sensitivity to high temperatures (Halaharvi *et al.*, 2020). Risk also increases for those who live alone, have pre-existing illnesses, and/or live without cooling.

Children are also physiologically susceptible to heat exposure (Fujii and Honda, 2023). A series of studies show that temperatures over 40°C are positively associated with childhood stunting (Bharti *et al.*, 2019). In Varanasi, children in the age group 0–4 years have the highest relative mortality risk (Singh *et al.*, 2019). In a study on indoor thermal comfort of 12 primary school buildings in Dehradun City, Uttarakhand, India, during the summer of 2019, Lala *et al.* (2022) found that about 95% of students were studying at thermal conditions over 32.7°C, or in Heat Index terms, a heat risk labelled as "extreme caution" or "danger".

In the context of heatwaves in Odisha State, Patel *et al.* (2018) highlight narratives from local students that it was very difficult to conduct a class after 9am, because of high indoor temperatures (buildings made of concrete), and because of the limited number of fans available. This resulted in changing school hours to avoid peak heat hours (Patel *et al.*, 2020).

7.2 Household coping strategies

Structural adaptation strategies focus on increasing buildings' cooling potential. These can include new or retrofitted building materials such as brick, bamboo, straws or mud for walls, floors, and rooftops,

https://doi.org/10.25561/104092

adding more windows, or setting up a rooftop garden (Tawsif, Alam and Al-Maruf, 2022). In Ahmedabad, the first Indian (and South Asian) city to implement a Heat Action Plan, the Mahila Housing Trust has installed four different kinds of cool roofs in households in informal settlements to lower heat stress. They are the (i) modular roofing system (Mod Roof), which is a waterproof roofing, made of paper waste and coconut husk, easily installable which is helpful for slum dwellers if they shift elsewhere; (ii) airlite ventilation which involves installing fibre-made ventilation sheets on the roof that has a passage to allow daylight and airflow into the house; (iii) ceilings coloured white for reflecting sunlight; and (iv) thermocol ceilings, which have thermal insulating qualities and improves the sustainability by reducing expenditure on energy (Vellingiri *et al.*, 2020). In the densely populated city of Rajshahi, Bangladesh, 48.3% of household respondents indicate residing in *pacca* housing made entirely of bricks and 45% have cooling facilities such as fans and air conditioners, whereas 26.6% are lacking structural adaptation strategies altogether (Tawsif, Alam and Al-Maruf, 2022). Research on community coping strategies in rural Maharashtra, India, identifies ceiling (67%) and table fans (13.5%) as the most common heat-mediating measures (Pradyumna *et al.*, 2018). In a 2015 study, as little as 12% of women construction workers had access to fans and air conditioners; that is 29% lower than their male peers (Dutta *et al.*, 2015).

Active cooling devices, powered by electricity, can increase power demand and cause energy shortages (Wired, 2023; Rediff, 2023; Oilprice.com, 2023; Gulf News, 2023). Continuing to upscale the systematic implementation of passive cooling technologies in buildings remains critical to reduce household heat risks (see e.g. Lu *et al.*, 2022).

People's temporary behavioural changes can also reduce heat risk. For example, in urban slums in Kolkata, and rural areas of West Bengal, India, elderly village residents reported reducing household and economic activities, altering and reducing social activities, taking a shower or bath, moving to a cooler location, eliminating food items considered to be inappropriate for the heat, changing or removing clothing, and increasing water consumption (Mukhopadhyay and Weitz, 2022). However, using electric fans in sleeping areas at night and adding food items considered to be appropriate for the hot weather were significantly less common in the rural villages than in urban Kolkata slums (Mukhopadhyay and Weitz, 2022). Rural communities in Pune, Maharashtra, increase their drinking water consumption, use electric fans, sit under trees, reduce outdoor activities, and stay updated about heat stress information from radio/TV news. The use of fans, however, is less prevalent among the tribal population with lower income groups (Pradyumna *et al.*, 2018).

In Rajshahi, Bangladesh, behaviour related strategies include sitting beside water bodies, wearing comfortable clothes, opening windows or closing them during extreme heat periods (Tawsif, Alam and Al-Maruf, 2022). In Bangladesh, however, there is evidence of discriminatory social and cultural norms reducing women's adaptive capacity, such as needing male company to enjoy public spaces (Ferdous and Mallick, 2019; Ehsan *et al.*, 2021). Throughout the April heatwave, newspapers described these coping strategies as frequently deployed (The Daily Star, 2023; VOA News, 2023).

Factors such as education, household income, gendered norms, and risk perceptions also play an important role in determining behavioural responses (Adegun *et al.*, 2021). A recent study on heat risk perceptions of workers across India found less than 50% to be aware of personal coping strategies and identified the need to increase worker awareness (Latha *et al.*, 2022). On the other hand, another study found most adaptation methods are adopted merely based on economic feasibility across workers in the informal sector (Kotharkar *et al.*, 2022). This highlights the inequality in heat adaptation across socio-economic lines and the need for protection through policies and legislation.

7.3 Informal housing and urban planning for heat

Informality is a key feature in urban areas worldwide. Informal and semi-informal settlements are known with different names across the world such as slums, bastis, favelas etc. In the context of the ongoing heatwave, while heat is known to most places in South Asia, the current pattern of heatwave impacts is alarming due to the scale of insecure living and working conditions (Zachariah *et al.*, 2022). Household construction materials, such as tin sheets, exacerbate heat risk. A number of heat action plans and studies in India recognise the disproportionate impacts of heat on those living in informal settlements (Chu and Micheal, 2022; Raju, Boyd and Otto, 2022). The social, political and economic determinants of living in informal settlements such as insecure land tenure, security, limited access to public services such as healthcare, water, and energy, combined with individual barriers associated with age, gender, income, and occupation lead to various exacerbated impacts (Hambrecht *et al.*, 2022). A study in Kolkata in India found that coping and adaptive mechanisms were driven more by the availability of resources and socio-cultural and political contexts than heat-related metrics and thresholds (Mukhopadhyay and Wietz, 2022).

In Lao PDR, for example, as of 2020, about 22% of the urban population lives in slums (The World Bank, 2023). While not all who live in precarious housing conditions work in the informal economy, heat-health risks are exacerbated when this pattern materialises (Dodaman *et al.*, 2022). For example, home-based work available to many slum residents, such as cigarette making (commonly known as Beedi in South Asia) already has negative health impacts (Coburn and Sverdlik, 2018, Barman and Sarkar, 2022).

Unhoused populations are also at risk. In Bangkok, Thailand, it is estimated that the number of homeless people has risen by about 30% during the Covid-19 pandemic (ThaiHealth, 2022). In Delhi, there are winter relief programs for homeless people, but these programs are inadequate and do not seem to exist for extreme heat (HLRN, 2023).

It must be highlighted that initiatives such as nature-based solutions offer many opportunities to tackle and minimise heat impacts. Examples from cases in South-East Asian countries such as Thailand's informal settlements include community gardens, green spaces, and understanding them as more than mere physical-infrastructural projects. That is to recognise the co-benefits of nature-based solutions as a linkage across "social-ecological-technological systems" (Wolff, Rauf and Hamel, 2023).

Urban Heat Islands (UHI) have been observed in many cities in South Asia, such as in Dhaka, Bangladesh (Mani *et al.*, 2018) and in Bangkok, Thailand (Marks and Connell, 2023). South and Southeast Asia are home to the world's largest and third-largest annual increases in heat exposure, respectively, with India and Bangladesh ranking 1 and 2 and Thailand ranking 6 among countries globally (Tuholske *et al.*, 2021). These increases are overwhelmingly driven by population growth. One of the region's megacities, Dhaka is especially at risk from extreme heat events that have adverse effects on living standards and conditions, and is known as one of the worst-affected places by urban heat globally (Tuholske *et al.*, 2021). Most vulnerable groups who are highly exposed to extreme heatwave risk experience significant damage to their health. Bangkok's UHI is a result of lack of green space, high levels of air conditioning, and high rates of exhaust fumes. High rates of exhaust fumes in Bangkok amplify the effects of heatwaves by exacerbating air pollution. Bureaucratic inertia, fragmentation and divisions within government, and a focus on profiteering from rapid development have significantly compounded the UHI effect in Bangkok which greatly worsens the effects of heatwaves (Marks and Connell, 2023).

7.4 Heatwave Action Planning, Preparedness, and Response

7.4.1 Heat Action Planning

Heat Action Plans (HAPs) are a critical adaptation measure to manage heat risk, notably as a pathway to institutionalise preparedness and response for heatwaves and securing habitability (Horton *et al.*, 2021). Aimed at alerting at-risk populations and other residents of extreme heat and guiding them in taking appropriate precaution, HAPs provide a framework for implementing, coordinating, and evaluating responses to heatwaves.

7.4.1.1 Heat Action Plans: India

India's National Disaster Management Plan recognises heatwaves as one of the meteorological hazards. In 2019, the National Disaster Management Authority (NDMA) issued guidelines for states to prepare their HAPs (NDMA, 2019). However, cities like Ahmedabad and states such as Odisha have been proactive and introduced HAPs and strategies to address heatwave prior to NDMA's guidelines (NRDC, 2022). According to the guidelines, the development of the HAP was recommended to be an eight-step long process: setting up a state-level committees including all the major stakeholders, appointing nodal agency/officers for preparing the HAP, assessing vulnerability and establishing heat-health temperature thresholds, drafting and developing the Plan, preparing and coordinating response, implementing and monitoring the Plan, and lastly, evaluating and updating the Plan (NDMA, 2019).

While the NDMA Guidelines call for a vulnerability assessment, it does not provide a framework besides indicating examples of physically vulnerable population groups (NDMA, 2019). Interestingly, a recent review of the 37 HAPs developed at state, district, and city level shows that nearly all have an oversimplified view of heatwaves, and many do a poor job at identifying and targeting vulnerable groups, including taking into account the intersecting dimensions of inequality (Pillai and Dalal, 2023). This is certainly the case for migrant workers and informal settlers in India whose marginal existences, basic needs, and limited political representation and negotiating power are barely reflected in often technocratic approaches to heat risk management and urban planning (Chu and Michael, 2019). Pillai and Dalal (2023) moreover found that those HAPs that were based on a robust vulnerability assessment did not always follow through with targeted interventions. The homogenization of vulnerable groups observed in these HAPs masks structural and intertwined causes of differential vulnerability that prevent large portions of affected populations to effectively protect themselves by undertaking adaptive and preventive action. Generic recommendations to 'address vulnerable groups' and develop heat vulnerability indices for 'high-risk subgroups' to facilitate community adaptation (Sharma *et al.*, 2022) tend to perpetuate socio-cultural blind spots. As shown in the often acclaimed HAP for Ahmedabad, India, many disadvantaged and most vulnerable target groups remain excluded and, as a compounding effect of highly uneven urban development, are left without safeguards and without timely and committed disaster relief (Nastar, 2020). Equally detrimental are ill-designed information-dissemination campaigns that fail to reach the most disenfranchised members of society, precisely due to layered patterns of social and political discrimination, and typically don't offer measures to address barriers of unequal access to health services, cooling strategies and spaces, and/or financial support, for instance to purchase water or cooling devices (Pillai and Dalal 2023).

7.4.1.2 Heat Action Plans: Thailand and Lao PDR

Despite recurring and deadly heatwaves in the region, neither Thailand nor Lao PDR have a HAP in place. However, during the last week of April, Thai authorities advised people in Bangkok and other areas of the country to stay home to avoid exposure to the extreme heat (AP News, 2023). Extreme heat does figure in Thailand's National Disaster Management Plan but it is mostly indicative of what constitutes heatwaves in the local context and which regions are likely to experience it (CFE-DM, 2022). HAPs were not identified for Lao PDR and the Disaster Management Plan does not refer to extreme heat (CFE-DM, 2021). The severity and complexity of heatwaves experienced in this region, coupled with a lack of guiding documents for preparedness and action, are likely to exacerbate the impacts on vulnerable communities.

7.4.1.3 Heat Action Plans: Bangladesh

A number of studies have found high heat-related mortality during recent heatwave events in Bangladesh, and an Early Action Protocol (EAP) has been piloted with cash transfers given to poor residents in Dhaka in advance of a heatwave event (Nissan *et al.*, 2017; Arrighi *et al.*, 2017, Anticipation Hub). Further, the city of Dhaka recently announced a Chief Heat Officer, the first of its kind in an Asian city, to lead efforts to reduce heat-related risks (One Billion Resilient, 2023). While there is currently no HAP in place, there have been discussions to develop them for heat-prone cities like Rajshahi (Khan, R. and Blackwell, C. 2022).

7.4.2 Early Warning Systems

In most countries, the respective national meteorological agency is responsible for forecasting hazards and disseminating information to relevant stakeholders through various channels. In India, the Indian Meteorological Department (IMD) indicated on April 8th that there would be a gradual rise in maximum temperature by 2-4C over most of the country over the subsequent 5 days. On April 13, IMD issued a "Watch" for heatwave conditions over Gangetic West Bengal, Odisha, Coastal Andhra Pradesh and Bihar (IMD). On April 18th, the heatwave watch was expanded to additional states in the north and east of the country, with Andhra Pradesh, West Bengal, and Bihar upgraded to "Alert" level, indicating the need to "be prepared" (IMD). Furthermore, the National Disaster Management Agency (NDMA) in India shared information on what to do during the heatwave to stay safe, including for school children, the elderly, and outdoor workers (NDMA, 2023).

In Bangladesh, the Bangladesh Meteorological Department also issues daily weather forecasts for various parts of the country, as well as Heatwave Warnings, but it is unclear whether a warning was issued for this event, as there is no record of one available on the website. The Bangladesh Red Crescent has conducted a feasibility study for developing an Early Action Protocol for heatwaves in Dhaka, but the protocol is currently still being developed and was not operational during this heatwave event (BRCS).

In Thailand, the Thai Meteorological Department (TMD) is responsible for issuing daily weather forecasts which includes minimum and maximum temperatures, while the Department of Disaster Prevention and Mitigation often issues heat-specific warning messages (TMD). In 2020, a real-time Heat Illness Alert System (HIAS) was tested in Thailand, and it can provide real-time heat illness risk warning (Kirtsaeng and Kirsaeng, 2020). During the studied event, the Department of Disaster Prevention and Mitigation issued warnings that temperatures would exceed 40°C in several provinces, and warned against going outdoors during the heat (Reuters, 2023). However, many heat-related deaths happen indoors, when people live in uninsulated homes with no means to cool them.

https://doi.org/10.25561/104092

The Lao PDR has a Department of Meteorology and Hydrology which issues short, medium and long-range forecasts, but specific warnings for extreme heat do not appear to be issued (DMH). Given this, it is clear that there are some warnings issued in the region, but there are also gaps in early warning system coverage that can be filled to reduce the impacts of future heatwave events. Further, robust, localised temperature thresholds that include health-relevant variables such as humidity and/or night-time temperature are required in order to calibrate the warning system to potential local impacts (McGregor *et al.*, 2015).

7.4.3 Response

The extreme heat prompted a range of responses by governmental authorities in order to reduce risks and impacts from the extreme heat. Across India, various responses from governmental authorities were reported. In Orissa, the district administration allowed different urban and rural public spaces as shelters for homeless people (Outlook India, 2023). Moreover, district administrations were asked to take efforts to ensure sufficient water and other relief items such as oral rehydration solutions were available (The New Indian Express, 2023). Schools were closed in West Bengal, Tripura, and Odisha, and closed during the afternoons in Delhi (The Guardian, 2023). In some states, government offices were only open between 7 am and 1 pm (Arab News, 2023). In Karnataka, India's leading state for the production of clean energy, three coal power plants were required to run at maximum capacity to cope with the increased demand in electricity (The Japan Times, 2023). Furthermore, The Ministry of Labor issued an advisory to all states to prioritise the safety of workers (particularly those who work outdoors and in mines) and to provide adequate drinking water, emergency ice packs, and frequent rest breaks (The Economic Times, 2023). It is unclear to what degree employers implemented these recommendations.

At the same time, a lack of appropriate response can aggravate impacts from the heat. On April 16, the state government of Maharashtra in India organised an award ceremony, anticipating 1.5-2 million people to attend on a public open ground. The timing of the event was during the hottest period of the day. Despite arrangements for drinking water and medical aid, not everyone could access it, resulting in about 650 emergency admissions and 13 deaths (Mint, 2023; Scroll, 2023). This event raised concerns around the need for (stricter) regulations and procedures during public events.

In Bangladesh, the Bangladesh Rice Research Institute (BRRI) issued a warning to farmers to ensure their rice fields were sufficiently irrigated during the extreme heat, but advice this may be challenging as it could increase their exposure to the heat (Al-Masum Molla, 2023). The Department of Agricultural Extension provided guidelines on how to protect crops and fruits (The Business Standard, 2023). Across Thailand and Lao PDR, no governmental responses were found to be reported at the time of writing.

7.5 V&E Conclusion

In addition to the hazard itself, there are many factors that made people more susceptible and exposed to the hot temperatures and humidity in early April 2023. Compounding factors, both biophysical (e.g. pre-existing medical conditions) and social (e.g. poverty, social discrimination on the basis of caste or religion, etc.), amplify the impacts of heat stress on exposed and vulnerable populations and hence exacerbate harm experienced. In addition, air pollution, wildfires, and urban heat islands can also amplify the health risks associated with high temperature. In each of the countries studied, the people who are most vulnerable vary based on the respective societal make-up, and in some cases are driven by deep rooted, systemic inequalities. Therefore, it is critical to address the underlying root causes of vulnerability as events like this one become more frequent in the future.

While early warnings were sent out on the heatwave (especially in India), it is not clear whether they arrived early enough to allow people adequate time to prepare in advance, as the majority of action was taken once the heat and humidity had already arrived. Early warning systems for heat can be strengthened, especially in places where they are in their infancy or don’t currently exist (Lao PDR), including by adding relevant variables that lead to adverse health outcomes like humidity and nighttime temperature, and connecting to local Heat Action Plans. The majority of literature on Heat Action Plans comes from India, where this strategy has been most widely implemented. In India, a lack of vulnerability assessment frameworks limits current Heat Action Plans from truly addressing the needs of those who are most vulnerable, and improvement in this area can help to make current plans more effective. A regionally transferable framework for vulnerability assessments could also help to spread HAPs to other countries in South and Southeast Asia.

Households and individuals often find ways to cope by using fans, evaporative coolers, taking more showers, staying indoors during the hottest times of day and increasing water intake, for example. These self-protective behaviours, although often not available to the most disenfranchised populations, should be encouraged and shared by authorities, along with information on recognising the signs of heat-related illness so that first aid or other appropriate action can be taken to save lives. When temperatures exceed certain thermal limits, however, it can be difficult to cool down without active cooling (air conditioning) which can strain the electrical grid leading to power outages, and again, access is inequitably distributed, meaning those most vulnerable continue to experience most harm. With heatwaves like this one becoming more frequent and intense, it will be important to better comprehend systematic inequalities and multidimensional vulnerabilities and how they interact with heat exposure, avoid reinforcing existing patterns of exclusion (e.g. regarding decision-making processes for heat action plans), ensure easier and timely access to water and medical assistance, and co-develop innovative solutions (e.g. group-specific early warning methods, shading structures, low-cost and locally produced cool roofs) that work for people in highly exposed contexts.

Data availability

Almost all data will be made available via the Climate Explorer.

IMD Gridded 1° x 1° Daily Maximum Temperature available here
https://www.imdpune.gov.in/cmpg/Griddata/Max_1_Bin.html
IMD Gridded 0.5° x 0.5° Daily Maximum Temperature available here
https://www.imdpune.gov.in/cmpg/Realtimedata/max/Max_Download.html

Supplement

https://doi.org/10.25561/104092

Table S1: Evaluation results of the climate models considered for attribution analysis of the April 4-day maximum Tx over the IB region. The table consists of qualitative assessments of the seasonal cycles and spatial patterns, the sigma and shape parameters from fitting a GEV distribution that shifts with GMST, and the effective return level of a 1-in-10 year event in the 2023 climate.

Observations	**Seasonal cycle**	**Spatial pattern**	**Sigma**	**Shape parameter**	**Event magnitude [°C]**
ERA5			1.05 (0.822 ... 1.22)	-0.35 (-0.51 ... -0.22)	
CPC			0.857 (0.601 ... 1.04)	-0.43 (-0.67 ... -0.20)	
Model					**Threshold for 10-year return period[°C]**
CMIP6 ()					
ACCESS-CM2_r1i1p1f1 ()	good	good	0.670 (0.380 ... 0.880)	-0.16 (-0.37 ... 0.34)	40.67
ACCESS-ESM1-5_r1i1p1f1 ()	good	bad	0.980 (0.670 ... 1.39)	-0.45 (-1.1 ... -0.26)	41.17
CanESM5_r1i1p1f1 ()	good	good	0.820 (0.640 ... 1.20)	-0.31 (-1.1 ... -0.14)	42.33
EC-Earth3_r1i1p1f1 ()	good	good	0.860 (0.610 ... 1.11)	-0.37 (-0.78 ... -0.060)	40.56
EC-Earth3-Veg_r1i1p1f1 ()	good	good	0.850 (0.530 ... 1.03)	-0.26 (-0.64 ... -0.010)	40.6
FGOALS-g3_r1i1p1f1 ()	good	reasonable	0.650 (0.440 ... 0.810)	-0.32 (-0.68 ... -0.030)	39.94
GFDL-CM4_r1i1p1f1 ()	good	reasonable	1.02 (0.700 ... 1.41)	-0.50 (-1.1 ... -0.19)	39.18
GFDL-ESM4_r1i1p1f1 ()	good	reasonable	0.900 (0.680 ... 1.23)	-0.30 (-1.1 ... -0.12)	38.92
INM-CM4-8_r1i1p1f1 ()	good	good	0.710 (0.430 ... 0.910)	-0.31 (-0.51 ... 0.10)	37.43
INM-CM5-0_r1i1p1f1 ()	good	good	0.670 (0.560 ... 0.720)	-0.53 (-0.82 ... -0.47)	38.18
KACE-1-0-G_r1i1p1f1 ()	good	good	0.610 (0.470 ... 0.740)	-0.43 (-0.90 ... -0.27)	42.83
KIOST-ESM_r1i1p1f1 ()	bad	bad	1.21 (0.900 ... 1.60)	-0.43 (-1.1 ... -0.21)	50.66
MPI-ESM1-2-LR_r1i1p1f1 ()	good	good	0.910 (0.660 ... 1.17)	-0.37 (-1.0 ... -0.17)	38.69
MPI-ESM1-2-HR_r1i1p1f1 ()	good	good	1.05 (0.940 ... 0.950)	-0.75 (-1.0 ... -0.68)	39.83
MRI-ESM2-0_r1i1p1f1 ()	good	good	1.41 (1.05 ... 1.89)	-0.38 (-1.1 ... -0.22)	41.65
NorESM2-LM_r1i1p1f1 ()	good	good	0.900 (0.660 ... 1.23)	-0.22 (-0.66 ... 0.010)	38.63

https://doi.org/10.25561/104092

NorESM2-MM_r1i1p1f1 ()	good	good	1.06 (0.770 ... 1.49)	-0.37 (-1.1 ... -0.20)	39.38
HiResMIP ()					
HadGEM3-GC31-MM ()			1.08 (0.800 ... 1.35)	-0.46 (-1.1 ... -0.34)	41.63
MPI-ESM1-2-HR ()			1.37 (0.970 ... 2.12)	-0.44 (-1.1 ... -0.13)	39.76
CNRM-CM6-1-HR ()			1.14 (0.700 ... 1.47)	-0.40 (-0.72 ... -0.040)	40.95

Table S2*:* Evaluation results of the climate models considered for attribution analysis of the April 4-day maximum Tx over the TL region. The table consists of qualitative assessments of the seasonal cycles and spatial patterns, the sigma and shape parameters from fitting a GEV distribution that shifts with GMST, and the effective return level of a 1-in-10 year event in the 2023 climate.

Observations	**Seasonal cycle**	**Spatial pattern**	**Sigma**	**Shape parameter**	**Event magnitude [ºC]**
ERA5			1.09 (0.790 ... 1.27)	-0.34 (-0.54 ... -0.091)	
CPC			0.877 (0.662 ... 1.03)	-0.20 (-0.41 ... -0.037)	
Model					**Threshold for 10-year return period[ºC]**
CMIP6 ()					
ACCESS-CM2_r1i1p1f1 ()	good	good	1.24 (0.840 ... 1.69)	-0.48 (-1.1 ... -0.25)	38.33
ACCESS-ESM1-5_r1i1p1f1 ()	good	bad	0.810 (0.600 ... 0.960)	-0.24 (-0.69 ... -0.080)	43.71
CanESM5_r1i1p1f1 ()	good	good	1.70 (1.31 ... 2.39)	-0.46 (-1.1 ... -0.21)	39.72
EC-Earth3_r1i1p1f1 ()	good	good	1.21 (0.890 ... 1.56)	-0.47 (-1.1 ... -0.26)	39.23
EC-Earth3-Veg_r1i1p1f1 ()	good	good	1.63 (1.12 ... 2.03)	-0.32 (-0.67 ... -0.070)	39.32
FGOALS-g3_r1i1p1f1 ()	good	reasonable	0.940 (0.680 ... 1.39)	-0.34 (-1.1 ... -0.060)	39.58
GFDL-CM4_r1i1p1f1 ()	good	reasonable	1.79 (1.61 ... 1.61)	-0.85 (-0.77 ... -0.77)	38.98
GFDL-ESM4_r1i1p1f1 ()	good	reasonable	1.67 (1.50 ... 1.50)	-0.82 (-0.74 ... -0.74)	39.33
INM-CM4-8_r1i1p1f1 ()	good	good	1.33 (0.940 ... 1.86)	-0.10 (-0.78 ... 0.23)	33.69
INM-CM5-0_r1i1p1f1 ()	good	good	2.17 (1.57 ... 3.21)	-0.40 (-1.1 ... -0.20)	36.08

KACE-1-0-G_r1i1p1f1 ()	good	good	0.920 (0.640 ... 1.18)	-0.43 (-0.86 ... -0.21)	42.23
KIOST-ESM_r1i1p1f1 ()	bad	bad	0.900 (0.730 ... 0.990)	-0.49 (-0.77 ... -0.44)	49.19
MPI-ESM1-2-LR_r1i1p1f1 ()	good	good	1.64 (1.08 ... 2.46)	-0.60 (-1.2 ... -0.28)	37.96
MPI-ESM1-2-HR_r1i1p1f1 ()	good	good	1.05 (0.740 ... 1.56)	-0.43 (-1.1 ... -0.090)	39.65
MRI-ESM2-0_r1i1p1f1 ()	good	good	1.47 (1.02 ... 1.94)	-0.35 (-1.0 ... -0.050)	39.9
NorESM2-LM_r1i1p1f1 ()	good	good	0.810 (0.580 ... 1.00)	-0.48 (-0.76 ... -0.30)	36.66
NorESM2-MM_r1i1p1f1 ()	good	good	1.27 (0.850 ... 1.55)	-0.36 (-0.69 ... -0.13)	38.3
HiResMIP ()			(...)	(...)	
HadGEM3-GC31-MM ()			1.12 (0.700 ... 1.51)	-0.43 (-1.0 ... -0.090)	39.71
MPI-ESM1-2-HR ()			1.80 (1.40 ... 2.18)	-0.88 (-1.0 ... -0.44)	39.58
CNRM-CM6-1-HR ()			1.24 (0.970 ... 1.60)	-0.18 (-0.95 ... 0.010)	38.17

***Table S3**:* Probability ratio and change in intensity of Tx4d in the IB region, for models that passed the validation tests for (a) past vs. present and (b) present vs. future.

Model / Observations	**a. Past vs. present**		**b. Present vs. future**	
	Probability ratio PR [-]	**Change in intensity ΔI [˚C]**	**Probability ratio PR [-]**	**Change in intensity ΔI [˚C]**
ERA5	0.42 (0.045 ... 2.7)	-0.52 (-1.5 ... 0.50)		
CPC	5.5e+2 (0.33 ... ∞)	0.78 (-0.44 ... 1.9)		
ACCESS-CM2_r1i1p1f1 ()	25 (5.2 ... 1.0e+4)	1.0 (0.65 ... 1.4)	3.1 (2.4 ... 4.7)	0.60 (0.47 ... 0.75)
CanESM5_r1i1p1f1 ()	7.4e+3 (19 ... 1.0e+4)	1.4 (1.0 ... 1.9)	4.0 (3.1 ... 13)	0.80 (0.68 ... 0.92)
EC-Earth3_r1i1p1f1 ()	37 (2.7 ... 1.0e+4)	0.65 (0.20 ... 1.2)	2.1 (1.6 ... 2.8)	0.33 (0.18 ... 0.49)
EC-Earth3-Veg_r1i1p1f1 ()	4.4 (1.2 ... 37)	0.57 (0.060 ... 1.1)	1.7 (1.2 ... 2.6)	0.29 (0.070 ... 0.49)
FGOALS-g3_r1i1p1f1 ()	3.7e+2 (8.9 ... 1.0e+4)	1.1 (0.53 ... 1.6)	4.0 (2.9 ... 7.8)	0.70 (0.51 ... 0.90)

https://doi.org/10.25561/104092

GFDL-CM4_r1i1p1f1 ()	2.6 (0.37 ... 82)	0.27 (-0.32 ... 0.79)	2.7 (2.1 ... 3.7)	0.54 (0.29 ... 0.68)
GFDL-ESM4_r1i1p1f1 ()	0.97 (0.039 ... 54)	-0.010 (-0.89 ... 0.79)	1.8 (1.0 ... 3.1)	0.33 (0.010 ... 0.69)
INM-CM4-8_r1i1p1f1 ()	2.1 (0.27 ... 24)	0.27 (-0.49 ... 1.1)	2.9 (1.9 ... 4.2)	0.49 (0.24 ... 0.72)
INM-CM5-0_r1i1p1f1 ()	1.0e+4 (1.0 ... 1.0e+4)	0.61 (0.31 ... 0.82)	2.8 (1.0 ... 3.6)	0.57 (0.47 ... 0.73)
KACE-1-0-G_r1i1p1f1 ()	1.0e+4 (2.9e+2 ... 1.0e+4)	0.88 (0.54 ... 1.3)	3.2 (2.6 ... 4.0)	0.62 (0.56 ... 0.77)
MPI-ESM1-2-LR_r1i1p1f1 ()	3.2 (0.22 ... 1.0e+4)	0.43 (-0.40 ... 1.2)	0.88 (0.00010 ... 1.8)	-0.060 (-0.39 ... 0.31)
MPI-ESM1-2-HR_r1i1p1f1 ()	0.95 (0.99 ... 1.0e+4)	-0.010 (-0.42 ... 1.2)	0.94 (0.00010 ... 1.5)	-0.030 (-0.33 ... 0.27)
MRI-ESM2-0_r1i1p1f1 ()	0.69 (0.0030 ... 1.0e+4)	-0.23 (-1.6 ... 0.76)	2.0 (1.4 ... 3.1)	0.55 (0.16 ... 0.85)
NorESM2-LM_r1i1p1f1 ()	0.48 (0.096 ... 4.0)	-0.45 (-1.4 ... 0.68)	1.4 (0.60 ... 2.1)	0.16 (-0.19 ... 0.41)
NorESM2-MM_r1i1p1f1 ()	78 (2.9 ... 1.0e+4)	1.0 (0.28 ... 1.8)	2.5 (1.7 ... 4.0)	0.56 (0.23 ... 0.84)
HadGEM3-GC31-MM ()	1.0e+4 (1.0e+4 ... 1.0e+4)	1.7 (0.67 ... 2.7)	<not computed>	<not computed>
MPI-ESM1-2-HR ()	20 (0.42 ... 1.0e+4)	0.89 (-0.30 ... 1.9)	<not computed>	<not computed>
CNRM-CM6-1-HR ()	1.0e+4 (87 ... 1.0e+4)	1.6 (0.69 ... 2.7)	<not computed>	<not computed>

Table S4: Probability ratio and change in intensity of Tx4d in the TL region, for models that passed the validation tests for (a) past vs. present and (b) present vs. future.

Model / Observations	**a. Past vs. present**		**b. Present vs. future**	
	Probability ratio PR [-]	**Change in intensity ΔI [˚C]**	**Probability ratio PR [-]**	**Change in intensity ΔI [˚C]**
ERA5	5.2 (0.033 ... ∞)	0.23 (-1.1 ... 1.1)		
CPC	5.6 (0.31 ... ∞)	0.79 (-0.51 ... 2.2)		
	(...)	(...)		
ACCESS-CM2_r1i1p1f1 ()	12 (0.76 ... 1.0e+4)	0.74 (-0.16 ... 1.6)	3.6 (2.9 ... 5.3)	0.89 (0.66 ... 1.1)
EC-Earth3_r1i1p1f1 ()	15 (3.9 ... 1.0e+4)	1.2 (0.27 ... 1.9)	2.1 (1.7 ... 4.3)	0.62 (0.36 ... 0.97)

https://doi.org/10.25561/104092

FGOALS-g3_r1i1p1f1 ()	16 (0.92 ... 1.0e+4)	0.68 (-0.14 ... 1.4)	2.5 (1.8 ... 4.7)	0.46 (0.19 ... 0.78)
INM-CM4-8_r1i1p1f1 ()	2.7 (0.78 ... 7.2)	1.3 (-0.23 ... 2.4)	1.4 (1.1 ... 1.9)	0.51 (0.080 ... 0.88)
KACE-1-0-G_r1i1p1f1 ()	1.0e+4 (1.2 ... 1.0e+4)	1.3 (0.67 ... 1.4)	2.4 (1.0 ... 4.2)	0.76 (0.50 ... 0.75)
MPI-ESM1-2-HR_r1i1p1f1 ()	2.5 (0.047 ... 1.0e+4)	0.38 (-0.84 ... 1.3)	0.97 (0.38 ... 1.7)	-0.010 (-0.39 ... 0.33)
MRI-ESM2-0_r1i1p1f1 ()	2.6 (0.11 ... 1.0e+4)	0.63 (-0.87 ... 2.0)	2.4 (1.8 ... 3.4)	0.95 (0.37 ... 1.3)
NorESM2-LM_r1i1p1f1 ()	1.0e+4 (55 ... 1.0e+4)	1.3 (0.59 ... 2.0)	4.1 (3.2 ... 9.2)	0.94 (0.60 ... 1.4)
NorESM2-MM_r1i1p1f1 ()	1.0e+4 (1.0e+4 ... 1.0e+4)	2.4 (1.4 ... 3.5)	3.6 (2.6 ... 9.1)	1.0 (0.70 ... 1.3)
HadGEM3-GC31-MM ()	1.0e+4 (2.1e+2 ... 1.0e+4)	1.6 (0.66 ... 2.4)	<not computed>	<not computed>
CNRM-CM6-1-HR ()	6.9 (2.0 ... 1.0e+4)	1.5 (0.45 ... 2.5)	<not computed>	<not computed>

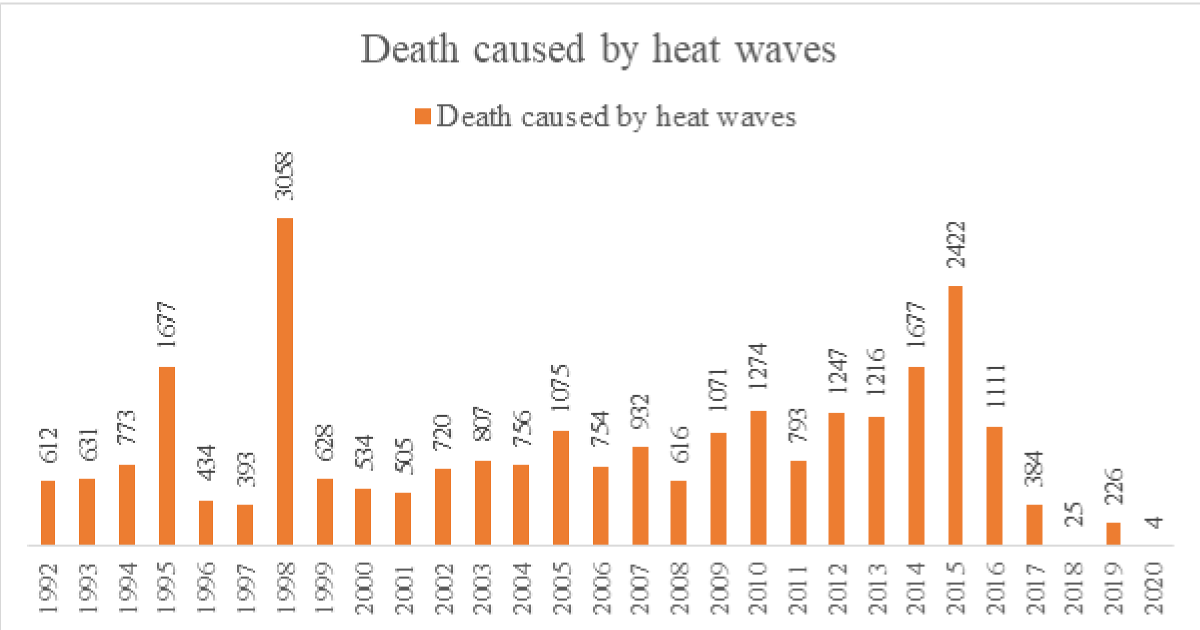

Figure S1: Death caused by heatwaves in India since 1992 Source: National Disaster Management Authority and National Institute of Disaster Management reports

https://doi.org/10.25561/104092

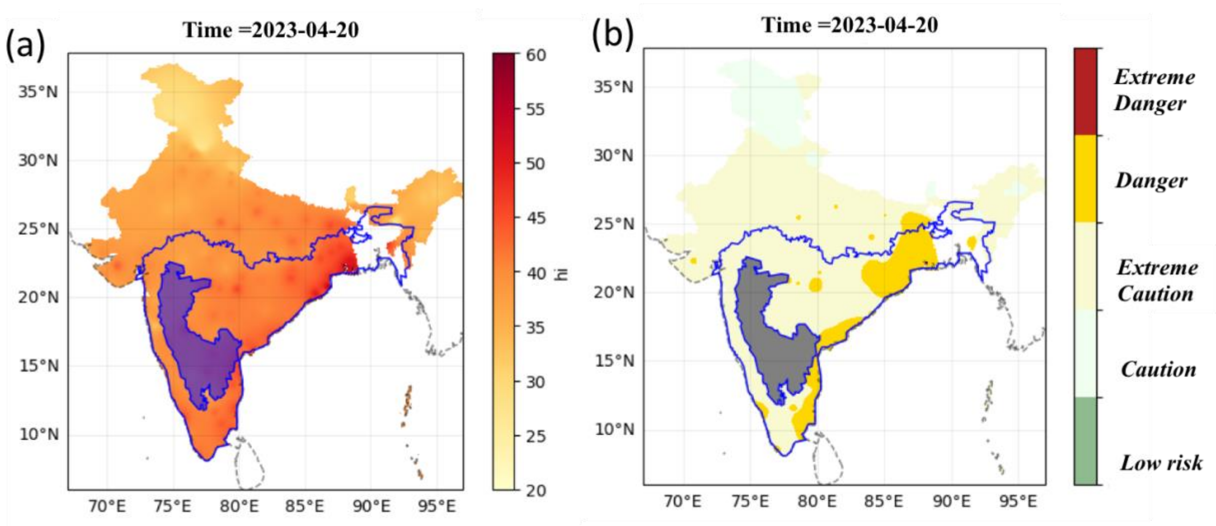

Figure S2: (a) Heat Index (calculated from IMD near-surface temperature and dew point temperature) [℃] showing 4-day average daily maximum for the period from 17th to 20th of April 2023 for India. (b) Classification maps for heat impacts based on HI, for the 4-day average daily maximum HI for the period from 17th to 20th of April 2023 for India.

https://doi.org/10.25561/104092

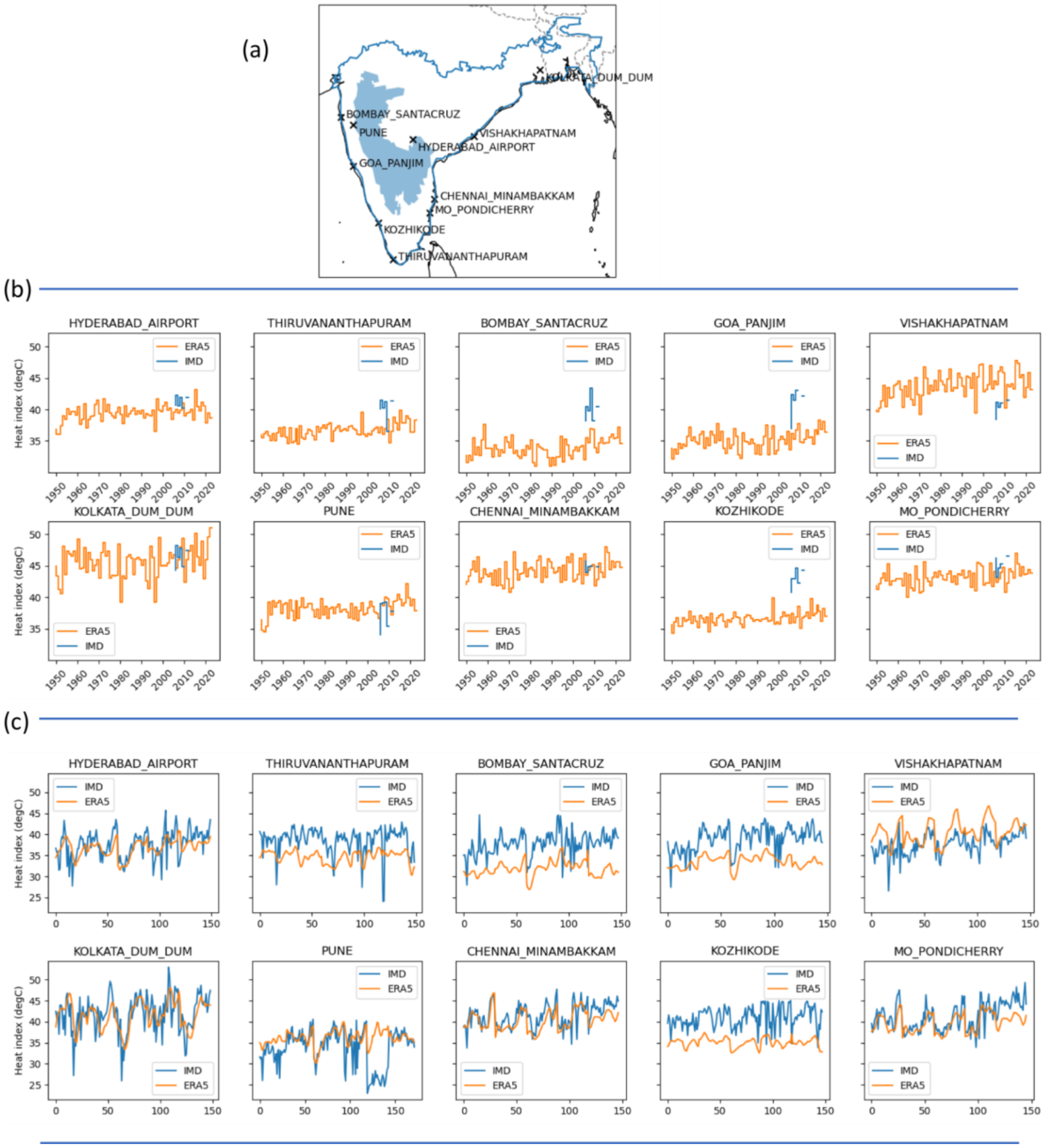

***Figure S3**:* (a) Locations of selected weather stations in the coastal regions of India at which HI is calculated for comparison with ERA5-based estimates. (b) Comparison between April HIx4d from the two datasets. (c) same as(b), for daily HI for all days in April, for the period 2006-2012.

https://doi.org/10.25561/104092

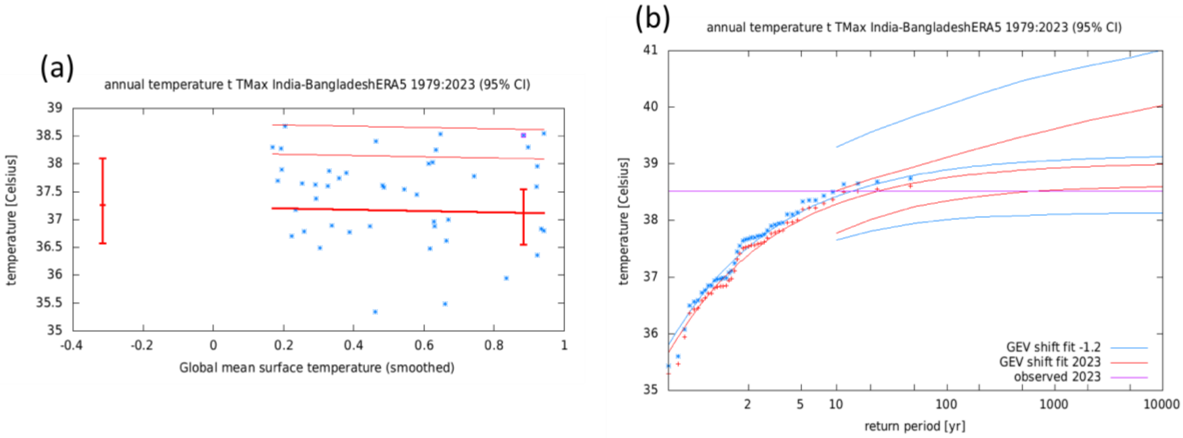

Figure S4: (a) Response of April Tx4d area-averaged over the IB region estimated from ERA5 records from 1979-2023 to change in global mean temperature. The thick red line denotes the time-varying mean, and the thin red lines show 1 standard deviation (s.d) and 2 s.d above. The vertical red lines show the 95% confidence interval for the location parameter, for the current, 2023 climate and the hypothetical, 1.2ºC cooler climate. The 2023 observation is highlighted with the magenta box. (b) Return periods for the 2023 climate (red lines) and the 1.2ºC cooler climate (blue lines with 95% CI), based on CPC data.

Acknowledgements

Lisa Thalheimer, *United Nations University, Institute for Environment and Human Security, Bonn, Germany*

Please cite this report as:

Zachariah, M; Vautard, R; Chaithra, S T; Kimutai, J; Arulalan, T; AchutaRao, K; Barnes, C; Singh, R; Vahlberg, M; Arrgihi, J; Raju, E; Sharma, U; Ogra, A; Vaddhanaphuti, C; Bahinipati, C S; Tschakert, P; Chandrasekaran, R; Pereira, C; Mondal, A; Schwingshackl, C; Philip, S; Otto, FEL (2023). Extreme humid heat in South and Southeast Asia in April 2023, largely driven by climate change, detrimental to vulnerable and disadvantaged communities.
DOI:https://doi.org/10.25561/104092.